EUROPEAN HEMATOLOGY ASSOCIATION
haematologica
Journal of the European Hematology Association

NIPBL: a new player in myeloid cells differentiation

by Mara Mazzola, Gianluca Deflorian, Alex Pezzotta, Laura Ferrari, Grazia Fazio, Erica Bresciani, Claudia Saitta, Luca Ferrari, Monica Fumagalli, Matteo Parma, Federica Marasca, Beatrice Bodega, Paola Riva, Franco Cotelli, Andrea Biondi, Anna Marozzi, Gianni Cazzaniga, and Anna Pistocchi

Haematologica 2019 [Epub ahead of print]

Citation: Mara Mazzola, Gianluca Deflorian, Alex Pezzotta, Laura Ferrari, Grazia Fazio, Erica Bresciani, Claudia Saitta, Luca Ferrari, Monica Fumagalli, Matteo Parma, Federica Marasca, Beatrice Bodega, Paola Riva, Franco Cotelli, Andrea Biondi, Anna Marozzi, Gianni Cazzaniga, and Anna Pistocchi. NIPBL: a new player in myeloid cells differentiation. Haematologica. 2019; 104:xxx doi:10.3324/haematol.2018.200899

NIPBL: a new player in myeloid cells differentiation

Mara Mazzola[1], Gianluca Deflorian[2], Alex Pezzotta[1], Laura Ferrari[2], Grazia Fazio[3], Erica Bresciani[4], Claudia Saitta[3], Luca Ferrari[1], Monica Fumagalli[5], Matteo Parma[5], Federica Marasca[6], Beatrice Bodega[6], Paola Riva[1], Franco Cotelli[7], Andrea Biondi[3], Anna Marozzi[1], Gianni Cazzaniga[3] and Anna Pistocchi[1]

[1]Dipartimento di Biotecnologie Mediche e Medicina Traslazionale, Università degli Studi di Milano, L.I.T.A., Segrate (MI), Italy.

[2] Istituto FIRC di Oncologia Molecolare, IFOM, Milano, Italy.

[3] Centro Ricerca Tettamanti, Clinica Pediatrica Università di Milano-Bicocca, Centro Maria Letizia Verga, Monza (MB), Italy.

[4] Oncogenesis and Development Section, National Human Genome Research Institute, National Institutes of Health, Bethesda, MD, USA.

[5] Haematology Division and BMT Unit, Ospedale San Gerardo, Monza (MB), Italy.

[6] Istituto Nazionale di Genetica Molecolare "Romeo ed Enrica Invernizzi" (INGM), Milan, Italy.

[7]Dipartimento di Bioscienze, Università degli Studi di Milano, Milano, Italy.

Statement of equal authors' contribution: M.M. and G.D.F. equally contributed to this work

Running head: *NIPBL*/*NPMc+* interplay in myeloid differentiation

Correspondence: Anna Pistocchi: anna.pistocchi@unimi.it

Abstract word count: 206

Main Text word count: 4015

Tables: 0

Figures: 6

Supplemental file: 1

Acknowledgements

We thank Monteiro R., (University of Birmingham), for the *Tg(CD41:GFP/kdrl:dsRED)* zebrafish line, N. Bolli, (University of Milan) for useful discussion of the data, the cytometry desk staff (IFOM, Milan) for technical help in FACS experiments, Crosti M.C. of the INGM FACS-sorting facility for sorting experiments and Spreafico M. and Cafora M. (University of Milan) for their priceless support in experimental procedures. This work was supported by the AIRC, Associazione Italiana per la Ricerca sul Cancro (MFAG#18714). The funders had no role in study design, data collection and interpretation, or the decision to submit the work for publication.

Abstract

NUCLEOPHOSMIN1 (NPM1) is the most frequently mutated gene in acute myeloid leukemia. Notably, *NPM1* mutations are always accompanied by additional mutations such as those in cohesin genes *RAD21*, *SMC1A*, *SMC3*, *STAG2* but not in the cohesin regulator *NIPBL*. In this work, we analyze a cohort of adult patients with acute myeloid leukemia and *NPM1* mutation and we observe specific reduction in the expression of *NIPBL* but not in other cohesin genes. In our zebrafish model, the overexpression of the mutated form of *NPM1* also induced the down-regulation of *nipblb*, the zebrafish orthologue of the human *NIPBL*. To investigate the hematopoietic phenotype and the interaction between mutated *NPM1* and *nipblb*, we generate a zebrafish model with *nipblb* down-regulation that shows an increased number of myeloid progenitors. This phenotype is due to a hyper activation of the canonical Wnt pathway: the rescue of myeloid cells blocked in an undifferentiated state is possible when the Wnt pathway is inhibited by *ddk1b* mRNA injection or indomethacin administration. Our results reveal for the first time a role for *NIPBL* during zebrafish hematopoiesis and suggest that *NIPBL*/*NPM1* interplay may regulate myeloid differentiation in zebrafish and humans through the canonical Wnt pathway and that dysregulation of these interactions may drive to leukemic transformations.

Introduction

Acute Myeloid Leukemia (AML) is a hematologic aggressive malignancy of bone marrow characterized by the accumulation of immature myeloid blasts defective in their differentiation and function.[1,2] The advances in cancer genomics results in the identification of relatively few recurrent somatic mutations giving rise to human AML, with an average of 5 mutations in each case of *de novo* AML.[3] These somatic mutations, that collectively determine the malignant phenotype, are serially acquired in clones of self-renewing hematopoietic stem cells (HSCs), termed pre-leukemic HSCs.[4] The gene mutated in HSCs that are relevant for AML pathogenesis have been divided in nine categories, including transcription-factor fusions, *NUCLEOPHOSMIN* (*NPM1*), tumor-suppressor genes, DNA-methylation–related genes, signaling genes, chromatin modifying genes, myeloid transcription-factor genes, cohesin-complex genes and spliceosome-complex genes.[5]

NPM1, the most frequently mutated gene in AML, is a phosphoprotein that normally resides into the nucleolus.[6,7] More than fifty different reported human mutations in *NPM1,* result in aberrant cytoplasmic translocation of the protein, named NPMc+, that functions as an oncogene *in vitro*[8] and has a role in aberrant hematopoiesis *in vivo*. Indeed, murine models expressing *NPMc+* in the hematopoietic lineage develop myeloproliferative disease[9] and leukemia[10,11] while the forced expression of human *NPMc+* in zebrafish causes an increase in primitive early myeloid cells and definitive hematopoietic stem cells (HSCs).[12,13] It has also been demonstrated, with similar results in zebrafish and human AML blasts, that the expression of *NPMc+* activates canonical Wnt signaling providing insight into the molecular pathogenesis of AML bearing *NPM1* mutations.[12] Indeed, the canonical Wnt/β-catenin pathway has been shown to be crucial for the regulation of HSCs proliferation, differentiation and apoptosis.[14]

Recently, it has been found a strong correlation between mutations in cohesin genes and *NPM1* mutations but they seem to not affect AML patient prognosis.[15] The cohesin complex is composed by different proteins that form a complex (SMC1, SMC3, RAD21, STAG1 and STAG2), and by

additional regulator proteins (NIPBL, MAU2, ESCO1, ESCO2 and HDAC8). This multifunctional complex regulates the cohesion of sister chromatids during cell division, but also gene transcription and chromatin architecture. Recently, the genes of the cohesin complex have been found mutated in almost 10% of patients with myeloid malignancies, while in an additional 15% of patients has been found a reduced expression of cohesin transcripts, suggesting a role for the cohesin-complex in the pathogenesis of AML.[5] In the patient cohort of Thota and colleagues [15], the most frequently mutated genes of the cohesin complex are *STAG2* (5.9%), *RAD21* (2%), and *SMC3* (2%), whereas mutations in the other cohesins are less than 1%. Somatic mutations in cohesin subunits are mutually exclusive and result in predicted loss-of-function phenotype being mainly nonsense and frameshift mutations.[16] It is to note that in AML neoplasms but not in other kind of tumors[17], cohesin mutations are associated with a normal karyotype in malignant cells, therefore the role for cohesins in the tumor development is not correlated with their function in sister chromatid cohesion rather than with their role in mediating DNA accessibility to gene regulatory elements.[15] Indeed, *in vitro* and *in vivo* models for cohesin haploinsufficiency display a delay in the differentiation of HSCs that are expanded in an immature state[18–21].

In this work, we have studied the expression of cohesin genes in a cohort of adult AML patients and found a specific down-regulation of *NIPBL* when *NPM1* is mutated. Interestingly, we found that also in our zebrafish model for *NPMc+* expression, *nipblb* was down-regulated. The zebrafish (*Danio rerio*) is a powerful model to study hematological diseases as it shares several hematopoietic genes with higher vertebrates, and mutations in human leukemia causative genes disrupt normal hematopoiesis in zebrafish, suggesting a functional conservation during evolution. Our zebrafish model with *nipblb*-loss-of-function showed dysregulation of myeloid cell differentiation with increased number of myeloid precursors and a decrease in myeloid mature cells. The hematopoietic phenotype presented by *nipblb*-loss-of-function zebrafish embryos recapitulated the myeloid defects presented by embryos with *NPMc+* overexpression and it was due to the hyper activation of the

canonical Wnt pathway. Indeed, the overexpression of the *dkk1b* Wnt inhibitor or by indomethacin treatment rescued the phenotype.

Our study provides new insights into the molecular mechanisms underlying *NIPBL* function, identifying the canonical Wnt pathway as one of its target and indicating it as a player with *NPMc+* in AML development. Using the well-suited zebrafish model, we established a platform to further investigate the mechanisms through which *NPMc+* and *NIPBL* might interact and contribute to leukemic transformation.

Methods

Patients

Bone Marrow (BM) diagnosis material of N=40 consecutive adult patients affected by AML or healthy subjects were collected and characterized as described in Supplementary Methods. Patient's material has been collected after obtaining Informed Consent ASG-MA-052A approved on May 8th 2012 by Azienda San Gerardo (ASG). Clinical features have been reported in Supplementary Table S1. Human material and derived data has been used in accordance with the Declaration of Helsinki.

Animals

Zebrafish (*Danio rerio*) embryos were raised and maintained according to international (EU Directive 2010/63/EU) and national guidelines (Italian decree 4th March 2014, n.26) on the protection of animals used for scientific purposes as described in Supplementary Methods.

Reverse transcription-PCR and real-time quantitative-PCR assays

Human and zebrafish embryos RNA extraction was performed using TRIZOL reagents (Life Technologies, Carlsbad, CA, USA), following the manufacturer's protocol. Quantitative RT-PCR experiments on human samples were performed with Universal Probe Library system (Roche Diagnostics, Basel, Swiss) as described in Supplementary Methods. Primers and probes are reported in Supplementary Table S2.

Western Blotting

Protein extracts were prepared, quantified and loaded as described in Supplementary Methods. Antibodies were listed in Supplementary Table S3. Imaging acquisition has been done with the Alliance MINI HD9 AUTO Western Blot Imaging System (UVItec Limited, Cambridge) and

analyzed with the related software.

In situ *hybridization and immunofluorescent analyses.*

Whole mount *in situ* hybridization (WISH) experiments, were carried out as described by Thisse and colleagues[22] and in Supplementary Methods. Picture were acquired with the photo camera Leica DFC480 (Leica, Wetzlar, Germany). Immunostaining was performed as described[23]. Antibodies list in Supplementary Table S3. Images were acquired as described in Supplementary Methods.

Sudan Black staining

Sudan Black staining was performed as described in[24] and in Supplementary Methods.

FACS analyses

Embryo dissociation was performed as described in[25]. FACS analysis were performed as described in Supplementary Methods from *Tg(CD41:EGFP)* zebrafish embryos at 3 dpf or Pu.1 stained cells derived from embryos at 3 dpf.

Injections and indomethacin treatment

Injections were carried out on 1- to 2-cell stage embryos. Morpholinos were injected as described in Supplementary Methods. Human *NPM1* and *NPMc+* and zebrafish *dkk1b* mRNAs were generated as previously described[12] and injected as described in Supplementary Methods. Indomethacin (indomethacin, Sigma-Aldrich) treatment was done as described in.[26]

Confocal imaging

Previously immunostained 3 dpf embryos were equilibrated and mounted in 85% glycerol solution in PBS and imaged using a "TCS-SP2" confocal microscope (Leica), with 40X oil immersion

objective, 488 nm argon ion and 405 nm diode lasers. For each sample, single stack images were acquired.

Statistical analyses

For RT-qPCR experiments, data were statistically analyzed applying one-way ANOVA- or t-tests, setting $p \leq 0.05$ (*), $p \leq 0.01$ (**), and $p \leq 0{,}001$ (***) as significant.[27] Data were analyzed using the comparative ΔΔCt method both t test and SD values refer to samples triplicates. In zebrafish at least three different experiments were done for each analysis. For cell count and phenotypical analyses, statistical analysis was performed by Chi square test, with Yates correction when needed.

Results

Cohesin expression in subgroups of adult AML patients carrying mutation in NPM1 *and in a zebrafish model of* NPMc+ *expression.*

Recently it has been reported that somatic mutations in cohesin genes are frequently associated with *NPM1* mutations[28], but not with other common AML mutations; however, the expression levels of cohesins has never been analyzed. Therefore, we decided to investigate the presence of alterations in the expression of cohesin genes in a cohort of N=40 adult AML patients stratified into two homogeneous molecular subgroups according to the absence or presence of *NPM1* mutation (*NPMc+*). Each subgroup was analyzed by means of RT-qPCR analyses for the expression of the cohesin genes: *SMC1A*, *SMC3*, *NIPBL* and *RAD21*(Figure 1A-D). Interestingly, only *NIPBL* showed a significant decreased expression in AML patients carrying *NPM1* mutation (Figure 1B). Conversely, when the same patients were divided into subgroups depending on the presence/absence of *FLT3/ITD* mutation, none of the cohesin gene analyzed was differently expressed between the two subgroups (Suppl. Figure S1).

We further analyzed by RT-qPCR the expression of cohesin genes in a zebrafish model with human *NPMc+* overexpression, previously generated and well characterized[12,13]. The injection of 100 pg/embryo of *NPMc+* transcript in zebrafish embryos, led to a significant down-regulation of *nipblb* in the whole embryo at 3 dpf, while the expression of other cohesin genes analyzed was unaltered or even increased (Figure 1E). We performed a stage-dependent analysis to dissect at which developmental stage the overexpression of *NPMc+* started to down-regulate *nipblb* expression in the whole embryo. We observed a significant decrease of *nipblb* expression starting from 48 hpf, while no decrease between controls and *NPMc+* mRNA injected embryos were observed at 24 and 36 hpf (Figure 1F). To further verify that the down-regulation of zebrafish *nipblb* was strictly dependent to the forced expression of *NPMc+*, we injected different doses of the *NPMc+* transcript (25 pg/embryo, 75 pg/embryo and 125 pg/embryo) and we showed a significant inverse correlation between *nipblb* reduced expression and *NPMc+* increase (Figure 1G). Moreover, by Western blot

analyses on embryos at 3 dpf, we confirmed that at the dose of 100pg/embryo, the injection of *NPMc+* mRNA determined a reduction of the Nipbl protein in comparison to control injected controls (Figure 1H).

nipblb-*loss-of-function and NPMc+ overexpression generates hematopoietic defects in zebrafish embryos*.

Since *NIPBL* is down-regulated in AML patients in association with *NPM1* mutation, we wonder whether *nipblb* knock-down might generate defects in myeloid cells differentiation. To investigate this hypothesis, we performed the down-regulation of *nipblb* in zebrafish by injecting a *nipblb* antisense oligonucleotide morpholino targeting the ATG region (*nipblb*-MO), as previously described for the knock-down of Nipbl protein[29,30]. In AML patients the HSCs and immature myeloid blasts are increased. Therefore, to screen for myeloid defects resembling AML patient conditions, we analyzed the same cell populations in *nipblb*-MO injected embryos. Knock-down of *nipblb* did not lead to significant differences in the HSCs, as shown by confocal images of the Caudal Hematopoietic Tissues (CHT) of *Tg(CD41:GFP)* embryos[31] at 3 dpf (Figure 2A-C) and by cytofluorimetric analyses (FACS) to quantify the CD41:GFP^{low} HSCs cells in comparison to controls (Figure 2G). On the other hand, at the same stage, *nipblb*-MO injected embryos showed an increase of myeloid progenitors, positive for the Pu.1 antibody (Figure 2H-I; FACS in K-L-N). These observations were also confirmed by means of Whole Mount *in situ*-hybridization (WISH) techniques with the HSC marker *cmyb* and the myeloid progenitor marker *spi1b* with relative quantifications of the observed phenotypes, and RT-qPCR analyses (Suppl. Figure S2). Moreover, to verify if the increased myeloid cells were blocked in an undifferentiated state, we performed a Sudan black staining to visualize mature myeloid cells[24]. At 4 dpf we observed a reduction of neutrophils (Figure 2O-P).

It has been previously reported that the forced expression of human *NPMc+* in zebrafish embryos increased HSCs population at 30-36 hpf[13]. To further analyze whether the hematopoietic defects are still present later during hematopoiesis and are extended to myeloid cells, we injected the embryos with *NPMc+* mRNA (100 pg/embryo) and analyze the hematopoietic phenotype. The CD41:GFP^{low} cells in the CHT of *NPMc+*-injected embryos were expanded in comparison to controls (Figure 2A-C; FACS in D-F-G), as well as the Pu.1 positive myeloid precursors (Figure 2H-J; FACS in K-M-N). Sudan black staining visualized a decrease in mature myeloid cells in *NPMc+* injected embryos in comparison to controls (Figure 2O-Q). Moreover, the expression levels of *cmyb* and *spi1b* were tested also by WISH and RT-qPCR techniques which corroborated our previous findings (Suppl. Figure S3).

To confirm the specificity of the hematopoietic defects obtained with *nipblb*-MO injection, we used a second morpholino targeting the 5'UTR region of *nipblb* (5'UTR*nipblb*-MO), previously used and validated[29]. The injection of this second morpholino reduced the Nipbl protein levels as observed by Western blot analyses, confirming its efficacy in blocking protein production. It also recapitulated the hematopoietic defects observed with the injection of the ATG morpholino, showing an increased number of myeloid precursors positive for *spi1b* and a decreased number of mature myeloid cells. Moreover, when co-injected at subcritical doses, the two *nipblb*-MOs cooperated to induce the myeloid phenotype (Suppl. Figure S4).

Nipbl *downregulation and* NPMc+ *overexpression both induce the hyper activation of the canonical Wnt pathway*

Previous experimental and clinical evidences suggested a close correlation between AML development and canonical Wnt pathway dysregulation, especially in patients with *NPM1* mutation[12]. To examine whether *nipblb* and *NPMc+* regulate the activation status of canonical Wnt pathway, we used the *Tg(TOPdGFP)* transgenic line that bears the GFP reporter gene under the control of four enhancers and the basal promoter of *lef1*, a β-catenin dependent transcription

factor[32]. *Tg(TOPdGFP)* embryos were injected with *nipblb*-MO or *NPMc+* mRNA and the expression of *gfp* and *axin2*, one of the direct targets of activated β-catenin, were analysed by RT-qPCR at 3 dpf[33]. Both genes were upregulated following both *nipblb* knock-down or *NPMc+* overexpression, indicating a hyper activation of the canonical Wnt pathway (Figure 3A-B). To determine whether the Wnt signaling was enhanced specifically in hematopoietic cells, confocal images of the CHT of *Tg(TOPdGFP)* embryos were analyzed (Figure 3C). GFP+ cells were increased either in *nipblb*-MO and *NPMc+* injected embryos (10 increased/10 scored). Specifically, *nipblb* down-regulation almost duplicated the number of GFP+ cells in the CHT (N=27±5) in comparison to controls (N14±3), (Figure 3D-E, quantification in I). Also *NPMc+* overexpression increased the number of GFP+ cells in the CHT (N=20±4) in comparison to controls (N=14±3), (Figure 3D-G, quantification in I). To further demonstrate that the increase of GFP+ cells in the CHT was due to hyper activation of the canonical Wnt pathway, we injected the Wnt inhibitor *dkk1b* mRNA (50 pg/embryo)[12]. We validated the efficiency of *dkk1b* mRNA injection as the GFP+ cells were diminished or absent in the hindbrain ventricle and in the CHT of the *Tg(TOPdGFP)* embryos in comparison to controls (Suppl. Figure S5). The co-injection of *dkk1b* in *nipblb*-MO or *NPMc+* mRNA injected embryos rescued the number of GFP+ cells in the CHT (10 rescued/10 scored for both) or even diminished the GFP+ cells (N=8±3 for *nipblb*-MO/*dkk1b*; N=10±3 for *NPMc+*/*dkk1b*) (Figure 3F-H, quantification in I). Moreover, using the Wnt reporter line *Tg(TOPdGFP)* we verified that, following *nipbl*-MO injection, the canonical Wnt pathway appeared downregulated at 24 hpf but was then hyper activated at 48 hpf (Suppl. Figure S6). This observation confirmed our previous work on a zebrafish model for *nipbl*-loss-of-function where we observed the dowregulation of the canonical Wnt pathway at 24 hpf and we correlated this with neurological defect presented by patients affected by Cornelia de Lange Syndrome (CdLS)[30].

Having seen a hyper activation of the canonical Wnt pathway in our zebrafish model with *nipbl* downregulation, we analyzed it also in AML human patients by measuring the expression of *AXIN2*, previously used as a reporter of canonical Wnt pathway activation in AML patients[12]. We

did not observe a significant increase in *AXIN2* expression in our cohort of AML patients with *NIPBL* downregulation (*NIPBL*<1) in comparison to those with normal or increased expression of *NIPBL* (*NIPBL*>1) (Suppl. Figure S7). Further analyses in major cohorts will be necessary to underline the correlation between *NIPBL* expression and canonical Wnt pathway.

Hyper activation of the canonical Wnt signalling in HSCs cells impairs myeloid differentiation.

To dissect which hematopoietic cell type in the CHT showed a hyper activation of the canonical Wnt pathway following *nipblb*-MO or *NPMc+* mRNA injections, we sorted the CD41:GFP^{low} cells (0.8% ctrl, 1% *nipblb*-MO, 1.1% *NPMc+*) from 3 dpf embryos injected with *nipblb*-MO or *NPMc+* mRNA and we observed a modest increase in *axin2* expression in comparison to CD41:GFP^{low} cells from controls (Figure 4A-A'''). Moreover, we performed immunofluorescence staining with the Active β-catenin (Active β-cat) antibody for the Wnt pathway and GFP antibody for HSCs cells of the CD41:GFP embryos. An increased number of double positive cells GFP/Active β-cat was present in the CHT of embryos at 3 dpf injected with *nipblb*-MO or *NPMc+* mRNA (5 double positive cells indicated by the arrows in the CHT of Figure 4C''-D'') in comparison to controls (2 double positive cells indicated by the arrows in the CHT of Figure 4B''), demonstrating that the Wnt pathway was activated specifically in HSCs cells (Figure 4B-D'').

The myeloid differentiation defects presented by *nipblb*-MO and *NPMc+* injected embryos at 3 dpf were caused by the hyper activation of the canonical Wnt pathway. In this regard, the inhibition of this pathway performed both with *dkk1b* mRNA injection or by treatment with the Wnt pharmacological inhibitor indomethacin,[26] rescued the hematopoietic phenotype. Indeed, by WISH we showed that the increased number of myeloid precursors positive for *spi1b* observed in *nipblb*-MO or *NPMc+* mRNA injected embryos, returned to levels comparable to controls (Figure 5A-G).

NPMc+ *and* nipblb *cooperation in the hyper activation of the canonical Wnt signaling and myeloid defects*

Our evidences so far showed that *NPMc+* down-regulates *NIPBL*, both in human AML patients and in zebrafish. We also demonstrated that dysregulation of both genes impairs myeloid differentiation through the hyper activation of the canonical Wnt pathway. To further address a possible cooperation between the two genes, we performed dose-response assays. We injected subcritical doses of *nipblb*-MO (0,6 pmol/embryo) or *NPMc+* mRNA (50 pg/embryo) that singularly did not cause an increased in GFP+ cells in the CHT of *Tg(TOPdGFP)* embryos or in the *spi1b* positive myeloid progenitors (Figure 6B-D) in comparison to controls (Figure 6A, quantification in E). When co-injected, subcritical doses of *nipblb*-MO/*NPMc+* recapitulated the phenotype previously observed by means of full doses injections, with an increased number of GFP+ cells in the CHT of the *Tg(TOPdGFP)* embryos and an enhanced expression of *spi1b* (Figure 6F-I, quantification of the phenotypes in J), indicating a cooperation between *NPMc+* and *nipblb* down-regulation.

Discussion

In this work, we rely on the observation that, in addition to the cohesin mutations detected in 10% of patients with myeloid malignancies, low expression of cohesin genes was present in an additional 15% of patients showing similar expression signatures as those with somatic cohesin mutations[28]. Therefore, we investigated the expression of cohesin genes in our cohort of 40 adult AML patients divided for the absence/presence of *NPM1* mutation. We chose to analyze *NPM1* mutations as they are pivotal in AML but likely insufficient by their self to cause malignant transformation, requiring the co-occurrence of other mutations such as *FLT3-ITD* or *RAS*[9,34]. In addition, it has been already reported a correlation between *NPM1* mutations and somatic mutations in cohesin genes,[28] but the specific loss-of-function of cohesins has never been investigated in association with *NPM1* mutations. Among the cohesin genes analyzed in our AML adult patient cohort, we found that only *NIPBL* showed a lower expression when *NPM1* was mutated. NIPBL is a regulator of the cohesin complex deputed to the loading of the complex onto the double-strand DNA. However, previous studies suggested a specific activity of NIPBL in gene transcription regulation and NIPBL binding sites, which do not overlap with those of cohesins, were *in vitro* identified.[35] Therefore, we decided to analyzed the effects of *NIPBL* down-regulation on myeloid differentiation. Zebrafish represents an ideal model for the study of cohesin genes function as it is possible to generate knock-down with the injection of specific oligonucleotide antisense morpholino.[30] Therefore, we investigate the effects of *nipblb*-loss-of-function during zebrafish definitive hematopoiesis and we observed an increased number of myeloid progenitors. Similar results have been obtained in different models of cohesins loss-of-function. For example, in murine models the use of shRNAs against *Stag2* and *Smc3* generated a maturation block, delayed differentiation, and enhanced renewal of HSCs, similar to myeloid neoplasms.[36] In another work, RNAi mouse models have created with inducible knock-down of *Rad21*, *Smc1a* and *Stag2* leading to a shift in the hematopoietic stem compartment, an increased replating capacity and, over time, the development of clinical features of

myeloproliferative neoplasms.[18] *NIPBL* is not a recurrently mutated gene in AML such as *STAG2*, *SMC3*, *SMC1A*, and *RAD21*.[28] In humans, heterozygous loss-of-function mutations of *NIPBL* cause the Cornelia de Lange Syndrome (CdLS).[37] Nevertheless, CdLS patients with mutations in *NIPBL* or in other cohesin genes are not predisposed to myeloid neoplasms. Rare cases of leukemia have been reported in CdLS probably caused by other physiological aspects of the pathology.[38–40] The mutations in cohesin genes responsible for CdLS and leukemia insurgence are considered different for their physio-pathological output: cohesin mutations in tumors occur in somatic an adult cells while germline cohesin mutations in CdLS patients occur in an embryonic tissue. Moreover, cohesin mutations in cancer might not trigger, but contribute to tumorigenesis only with other mutations such as *TET2*[41], *NPM1*[9,42], *DNMT3A*[43] or *FLT3-ITD*[44]. As a matter of fact, we speculate that the decrease in *NIPBL* expression observed in AML patients, might not be due to specific somatic mutations occurred at the gene level, rather than a secondary effect caused by genetic lesions arisen elsewhere (*i.e. NPM1*).

In *nipblb*-loss-of-function embryos we observed defects in myeloid differentiation with increased number of myeloid progenitors and decreased myeloid mature cells. These hematopoietic defects share similarities with the myeloproliferative phenotype of *NPMc+* embryos[12,13]. Indeed, we also confirmed that the forced expression of *NPMc+* generated a phenotype with an expansion of HSCs and myeloid precursors. However, the main difference in the hematopoietic phenotype generated by *nipblb* knock-down and *NPMc+* forced expression, was in the HSCs population. In this regard, while in *NPMc+* embryos the HSCs were significantly increased, in *nipblb*-MO injected embryos they were almost comparable to controls. This result is not surprising as we demonstrated that *nipblb* acts downstream of, and is regulated by, *NPMc+*. Therefore, it is conceivable that, also in the hematopoietic cascade that drives to myeloid differentiation, the effects of *nipblb* are directed on a population that derived from HSCs, such as myeloid progenitors.

We further observed that in *nipblb* knock-down and *NPMc+* overexpressed zebrafish embryos, the Wnt/β-catenin pathway was hyper activated. In the hematopoietic process many signaling pathways

are critical during different developmental stages of HSCs and for their maturation into differentiated lineages. In particular, the canonical Wnt pathway exerts its action on specific cell populations being fine-tuned in a dosage-dependent fashion[45]. We demonstrated that Nipbl is an active player in this modulation. Indeed, in a previous work, we showed that the downregulation of *nipblb* in zebrafish embryos at 24 hpf, caused a decreased activation of the canonical Wnt pathway[30]. In this work we demonstrated that, from 48 hpf, Nipbl acts in an opposite way by hyper activating the Wnt pathway in the whole embryo. It is conceivable that, given its double effects of on Wnt pathway, Nipblb might be considered a new player for canonical Wnt pathway modulation.

Recently several Wnt inhibitors have been identified as potential drugs to reduced tumor cell viability in lymphoma and myeloma cell lines *in vitro* and *in vivo*[46]. Thus, Wnt/β-catenin inhibitors, such as indomethacin that is already used in clinical trials[26] and is effective also in our study for the rescue of the hematopoietic phenotype, could be an attractive candidates for the development of new therapeutic treatments for *NPMc*+ AML patients.

Further analyses are necessary to investigate the mechanisms through which NPMc+ interact with *NIPBL* and they regulate the canonical Wnt pathway and the hematopoietic phenotype. One hypothesis that raised by previous and our analyses is the involvement of other members of the cohesin complex such as Rad21 that is negatively regulated by Nipbl both in murine fibroblast[47] and zebrafish (see Figure 1F). Alternatively, the aberrant cytoplasmic dislocation of mutant *NPM1* might alter the normal regulation of *NIPBL* expression in the nucleus, similarly to what happens in the important *PU.1*-NPM1 mediated regulation in myeloid precursors[48]. Large scale transcriptomic and/or proteomic analyses will be useful to unravel the mechanism and, at this purpose, the use of the zebrafish platform with cohesin knock-down might be a suitable model system.

In conclusion, our study correlates for the first time *NIPBL* with *NMP1* mutations in adult AML patients and demonstrates their interplay in myeloid cell differentiation in zebrafish throughout an involvement of the canonical Wnt pathway. The results obtained will foster the identification of new potential targets for treatments of AML subgroups.

References

1. Löwenberg B, Downing JR, Burnett A. Acute myeloid leukemia. N Engl J Med. 1999;341(14):1051–1062.
2. Ley TJ, Mardis ER, Ding L, et al. DNA sequencing of a cytogenetically normal acute myeloid leukaemia genome. Nature. 2008;456(7218):66–72.
3. Yan X-J, Xu J, Gu Z-H, et al. Exome sequencing identifies somatic mutations of DNA methyltransferase gene DNMT3A in acute monocytic leukemia. Nat Genet. 2011;43(4):309–315.
4. Corces-Zimmerman MR, Majeti R. Pre-leukemic evolution of hematopoietic stem cells: The importance of early mutations in leukemogenesis. Leukemia. 2014;28(12):2276–2282.
5. Voigt P, Reinberg D. Genomic and Epigenomic Landscapes of Adult De Novo Acute Myeloid Leukemia The Cancer Genome Atlas Research Network. N Engl J Med. 2013;368(22):2059–2074.
6. Borer RA, Lehner CF, Eppenberger HM, Nigg EA. Major nucleolar proteins shuttle between nucleus and cytoplasm. Cell. 1989;56(3):379–390.
7. Dumbar TS, Gentry GA, Olson MOJ. Interaction of Nucleolar Phosphoprotein B23 with Nucleic Acids. Biochemistry. 1989;28(24):9495–9501.
8. Cheng K, Grisendi S, Clohessy JG, et al. The leukemia-associated cytoplasmic nucleophosmin mutant is an oncogene with paradoxical functions: Arf inactivation and induction of cellular senescence. Oncogene. 2007;26(53):7391–7400.
9. Vassiliou GS, Cooper JL, Rad R, et al. Mutant nucleophosmin and cooperating pathways drive leukemia initiation and progression in mice. Nat Genet. 2011;43(5):470–476.
10. Alcalay M, Tiacci E, Bergomas R, et al. Acute myeloid leukemia bearing cytoplasmic nucleophosmin (NPMc+AML) shows a distinct gene expression profile characterized by up-

regulation of genes involved in stem-cell maintenance. Blood. 2005;106(3):899–902.

11. Mallardo M, Caronno A, Pruneri G, et al. NPMc+ and FLT3-ITD mutations cooperate in inducing acute leukaemia in a novel mouse model. Leukemia. 2013;27(11):2248–2251.
12. Barbieri E, Deflorian G, Pezzimenti F, et al. Nucleophosmin leukemogenic mutant activates Wnt signaling during zebrafish development. Oncotarget. 2016;7(34):55302–55312.
13. Bolli N, Payne EM, Grabher C, et al. Expression of the cytoplasmic NPM1 mutant (NPMc+) causes the expansion of hematopoietic cells in zebrafish. Blood. 2010;115(16):3329–3340.
14. Zhang J, Niu C, Ye L, et al. Identification of the haematopoietic stem cell niche and control of the niche size. Nature. 2003;425(6960):836–841.
15. Thota S, Viny AD, Makishima H, et al. Genetic alterations of the cohesin complex genes in myeloid malignancies. Blood. 2014;124(11):1790–1798.
16. Kagey MH, Newman JJ, Bilodeau S, et al. Mediator and cohesin connect gene expression and chromatin architecture. Nature. 2010;467(7314):430–435.
17. Solomon DA, Kim T, Diaz-Martinez LA, et al. Mutational inactivation of STAG2 causes aneuploidy in human cancer. Science. 2011;333(6045):1039–1043.
18. Mullenders J, Aranda-Orgilles B, Lhoumaud P, et al. Cohesin loss alters adult hematopoietic stem cell homeostasis, leading to myeloproliferative neoplasms. J Exp Med. 2015;212(11):1833–1850.
19. de Leval L, Waltregny D, Boniver J, Young RH, Castronovo V, Oliva E. Use of histone deacetylase 8 (HDAC8), a new marker of smooth muscle differentiation, in the classification of mesenchymal tumors of the uterus. Am J Surg Pathol. 2006;30(3):319–327.
20. Mazumdar C, Majeti R. The role of mutations in the cohesin complex in acute myeloid leukemia. Int J Hematol. 2017;105(1):31–36.
21. Fisher JB, Peterson J, Reimer M, et al. The cohesin subunit Rad21 is a negative regulator of hematopoietic self-renewal through epigenetic repression of Hoxa7 and Hoxa9. Leukemia. 2017;31(3):712–719.

22. Thisse C, Thisse B. High-resolution in situ hybridization to whole-mount zebrafish embryos. Nat Protoc. 2008;3(1):59–69.

23. Brusegan C, Pistocchi A, Frassine A, della Noce I, Schepis F, Cotelli F. Ccdc80-l1 is involved in axon pathfinding of zebrafish motoneurons. PLoS One. 2012;7(2):e31851.

24. Cvejic A, Serbanovic-Canic J, Stemple DL, Ouwehand WH. The role of meis1 in primitive and definitive hematopoiesis during zebrafish development. Haematologica. 2011;96(2):190–198.

25. Bresciani E, Broadbridge E LP. An efficient dissociation protocol for generation of single cell suspension from zebrafish embryos and larvae. MethodsX 2018;5:1287–1290.

26. North TE, Goessling W, Walkley CR, et al. Prostaglandin E2 regulates vertebrate haematopoietic stem cell homeostasis. Nature. 2007;447(7147):1007–1011.

27. Livak KJ, Schmittgen TD. Analysis of relative gene expression data using real-time quantitative PCR and the 2(-Delta Delta C(T)) Method. Methods. 2001;25(4):402–408.

28. Thol F, Bollin R, Gehlhaar M, et al. Mutations in the cohesin complex in acute myeloid leukemia: Clinical and prognostic implications. Blood. 2014;123(6):914–920.

29. Muto A, Calof AL, Lander AD, Schilling TF. Multifactorial origins of heart and gut defects in Nipbl-deficient zebrafish, a model of cornelia de Lange Syndrome. PLoS Biol. 2011;9(10):e1001181.

30. Pistocchi A, Fazio G, Cereda A, et al. Cornelia de Lange Syndrome: NIPBL haploinsufficiency downregulates canonical Wnt pathway in zebrafish embryos and patients fibroblasts. Cell Death Dis. 2013;4(10):e866.

31. Lin HF, Traver D, Zhu H, et al. Analysis of thrombocyte development in CD41-GFP transgenic zebrafish. Blood. 2005;106(12):3803–3810.

32. Dorsky RI, Sheldahl LC, Moon RT. A Transgenic Lef1/β-Catenin-Dependent Reporter Is Expressed in Spatially Restricted Domains throughout Zebrafish Development. Dev Biol. 2002;241(2):229–237.

33. Jho E, Zhang T, Domon C, Joo C-K, Freund J-N, Costantini F. Wnt/beta-catenin/Tcf signaling induces the transcription of Axin2, a negative regulator of the signaling pathway. Mol Cell Biol. 2002;22(4):1172–1183.

34. Dovey OM, Cooper JL, Mupo A, et al. Molecular synergy underlies the co-occurrence patterns and phenotype of NPM1-mutant acute myeloid leukemia. Blood. 2017;130(17):1911–1922.

35. Zuin J, Franke V, van IJcken WFJ, et al. A Cohesin-Independent Role for NIPBL at Promoters Provides Insights in CdLS. PLoS Genet. 2014;10(2):e1004153.

36. Galeev R, Baudet A, Kumar P, et al. Genome-wide RNAi Screen Identifies Cohesin Genes as Modifiers of Renewal and Differentiation in Human HSCs. Cell Rep. 2016;14(12):2988–3000.

37. Tonkin ET, Wang TJ, Lisgo S, Bamshad MJ, Strachan T. NIPBL, encoding a homolog of fungal Scc2-type sister chromatid cohesion proteins and fly Nipped-B, is mutated in Cornelia de Lange syndrome. Nat Genet. 2004;36(6):636–641.

38. Schrier SA, Sherer I, Deardorff MA, et al. Causes of death and autopsy findings in a large study cohort of individuals with Cornelia de Lange syndrome and review of the literature. Am J Med Genet A. 2011;155(12):3007–3024.

39. Deardorff MA, Bando M, Nakato R, et al. HDAC8 mutations in Cornelia de Lange syndrome affect the cohesin acetylation cycle. Nature. 2012;489(7415):313–317.

40. Vial Y, Lachenaud J, Verloes A, Besnard M, Fenneteau O, Lainey E, Marceau-Renaut A, Preudhomme C, Baruchel A, Cavé H DS. Down syndrome-like acute megakaryoblastic leukemia in a patient with Cornelia de Lange syndrome. Haematologica. 2018;103(6):274.

41. Moran-Crusio K, Reavie L, Shih A, et al. Tet2 Loss Leads to Increased Hematopoietic Stem Cell Self-Renewal and Myeloid Transformation. Cancer Cell. 2011;20(1):11–24.

42. Grisendi S, Bernardi R, Rossi M, et al. Role of nucleophosmin in embryonic development and tumorigenesis. Nature. 2005;437(7055):147–153.

43. Challen GA. Dominating the Negative: How DNMT3A Mutations Contribute to AML Pathogenesis. Cell Stem Cell. 2017;20(1):7–8.

44. Viny AD, Ott CJ, Spitzer B, et al. Dose-dependent role of the cohesin complex in normal and malignant hematopoiesis. J Exp Med. 2015;212(11):1819–1832.

45. Trompouki E, Bowman T V., Lawton LN, et al. Lineage regulators direct BMP and Wnt pathways to cell-specific programs during differentiation and regeneration. Cell. 2011;147(3):577–589.

46. Ma S, Yang LL, Niu T, et al. SKLB-677, an FLT3and Wnt/β-catenin signaling inhibitor, displays potent activity in models of FLT3-driven AML. Sci Rep. 2015;515646.

47. Newkirk DA, Chen YY, Chien R, et al. The effect of Nipped-B-like (Nipbl) haploinsufficiency on genome-wide cohesin binding and target gene expression: Modeling Cornelia de Lange syndrome. Clin Epigenetics. 2017;9:89.

48. Gu X, Ebrahem Q, Mahfouz RZ, et al. Leukemogenic nucleophosmin mutation disrupts the transcription factor hub that regulates granulomonocytic fates. J Clin Invest. 2018;128(10):4260–4279.

Figure Legends

Figure 1: Expression analyses of cohesin genes in AML adult patient Bone Marrow samples divided in two subgroups for the absence/presence of *NPM1* mutations and in a zebrafish model for *NPM1* mutation (NPMc+). *(A-D)* RT-qPCR analyses in N=40 AML adult patients indicated that the expression of *NIPBL* was decreased when *NPM1* was mutated. The other cohesin genes analyzed did not present a correlation with the presence of *NPM1* mutations. *(E)* RT-qPCR analyses of cohesin genes expression in a zebrafish model with overexpression of human *NPMc+*, showed that *nipblb* was down-regulated in comparison to controls at 3 dpf. *(F)* RT-qPCR time course analyses at 24, 36 and 48 hpf of *nipblb* expression in embryos injected with *NPMc+* transcript. *nipblb* was significantly down-regulated at 48 hpf. *(G)* RT-qPCR analyses of *nipblb* expression in zebrafish embryos at 3 dpf overexpressed with different doses of human *NPMc+*. The down-regulation of *nipblb* was significantly dependent to the *NPMc+* injection doses. *(H)* Western blot analyses of Nipbl protein expression in embryos at 3 dpf injected with 100 pg/ embryo of *NPMc+* transcript. Vinculin marker was used for normalization. Western blot images were processed as described in Supplementary Methods. Asterisks represent *= $p<0.05$, **= $p<0.01$ and ***=$p<0.001$ *(B, E, F, G, H).* ns: non-significant; AML: Acute Myeloid Leukemia; MO: morpholino; RT: Retro Transcription.

Figure 2: Myeloid cell differentiation is affected in *nipblb*-MO and *NPMc+* mRNA injected embryos. *(A, B, C)* Confocal analyses of *CD41:EGFP* HSCs of controls, *nipblb*-MO and *NPMc+* mRNA injected embryos at 3 dpf. The GFP positive HSCs cells were slightly increased in *nipblb*-MO, but significantly increased in *NPMc+* embryos in comparison to controls. *(D-G)* FACS analyses on GFP^{low} HSCs positive cells. *(H, I, J)* Confocal analyses of Pu.1 positive myeloid

precursor cells of controls, *nipblb*-MO and *NPMc+* mRNA injected embryos at 3 dpf. The GFP positive myeloid precursors cells were increased in both *nipblb*-MO and *NPMc+* embryos in comparison to controls. *(K-N)* FACS analyses on Pu.1 GFP positive cells. *(O-Q)* Sudan black staining for mature myeloid cells on controls, *nipblb*-MO and *NPMc+* mRNA injected embryos at 4 dpf. The mature myeloid cells were diminished in both *nipblb*-MO and *NPMc+* embryos in comparison to controls. Images were processed as described in Supplementary Methods. Scale bar represents 100 μm. Asterisks in *(G)* represent ***=p<0.001. ns: non-significant; HSCs: Hematopoietic Stem Cells; FACS: Fluorescence-Activated Cell Sorting; MO: morpholino; GFP: Green Fluorescent Protein; CHT: Caudal Hematopoietic Tissue.

Figure 3: Canonical Wnt signaling is hyper activated in *nipblb*-MO and *NPMc+ Tg(TOPdGFP)* injected embryos at 3 dpf. (A, B) RT-qPCR analyses of *gfp* and *axin2* expression in *nipblb*-MO and *NPMc+ Tg(TOPdGFP)* injected embryos indicated an increase of canonical Wnt activation status in comparison to controls. (C) Scheme of trunk-tail region of embryos. Confocal images were always performed in the same embryo region, comprising the tip of the yolk sack extension (YSE) between the dorsal aorta (DA, red line) and the vein (V, blue line) as indicated by pink brackets. *(D-H)* Confocal images of the CHT of *Tg(TOPdGFP)* embryos injected with *nipblb*-MO *(E)* and *NPMc+ (G)* showed an increase of GFP+ cells in comparison to controls *(D)*. The co-injection of the Wnt inhibitor *dkk1b* mRNA rescued the number of GFP+ cells *(F-H)*. *(I)* Quantification of GFP+ cells in the selected region of the CHT. Images were processed as described in Supplementary Methods. Scale bar represents 100 μm. Asterisks in *(A, B, I)* represent *=p<0.05, **=p<0.01 and ***=p<0.001. ns: non-significant; MO: morpholino; GFP: Green Fluorescent Protein; CHT: Caudal Hematopoietic Tissue.

Figure 4: Canonical Wnt pathway is hyper-activated specifically in HSCs cells.

(A-A'') FACS sorting of CD41:GFP^{low} cells from controls *(A)*, *nipblb*-MO *(A')* and *NPMc+* mRNA *(A'')* embryos at 3 dpf and RT-qPCR *axin2* expression analyses on sorted cells *(A''')*. *(B-D'')* Immunofluorescence staining with GFP for HSCs *(B, C, D)* and Active β-catenin for Wnt activation (Active β-cat) *(B', C', D')* antibodies. Merge of the two signals *(B'', C'', D'')* showed an increased number of double positive cells GFP/Active β-cat cells (arrows) in the CHT of embryos at 3 dpf injected with *nipblb*-MO or *NPMc+* mRNA in comparison to controls. Images were processed as described in Supplementary Methods. Scale bar represents 100 μm. Asterisk in *(A''')* represents *=p<0.05. ns: non-significant; HSCs: Hematopoietic Stem Cells; FACS: Fluorescence-Activated Cell Sorting; MO: morpholino; RT: Retro Transcription; GFP: Green Fluorescent Protein; CHT: Caudal Hematopoietic Tissue.

Figure 5: Myeloid cell differentiation impairment in *nipblb*-MO and *NPMc+* injected embryos is caused by hyper-activation of the canonical Wnt signaling. *(A-G)* WISH analyses of *spi1b*. The expression of *spi1b* was increased in *nipblb*-MO *(B)* and *NPMc+*-injected embryos *(E)* in comparison to controls *(A)*. Rescue of the myeloid phenotype was obtained with the injection of the Wnt inhibitor *dkk1b* mRNA *(C; F)* and with indomethacin treatment *(D; G)*. Quantifications of the observed phenotypes in *(H)* and *(I)*. Images were processed as described in Supplementary Methods. Scale bar represents 100 μm. Asterisks (*H* and *I*) represent *=p<0.05 and ***=p<0.001. MO: morpholino; WISH: Whole Mount In Situ Hybridization.

Figure 6: Co-injection of subcritical doses of *nipblb*-MO and NPMc+ that singularly do not have effects, indicates cooperation between *NPMc+* and *nipblb* in myeloid differentiation. *(A-D)* The number of GFP+ cells in the CHT was increased when embryos at 3 dpf were co-injected with subcritical doses of *nipblb*-MO/sub-*NPMc+ (D)* in comparison to single injection of a subcritical dose of controls *(A)*, *nipblb*-MO *(B)* and *NPMc+ (C)*. *(E)* Quantification of GFP+ cells in the CHT. *(F-I)* WISH analyses of the myeloid precursor marker *spi1b*. *spi1b* expression was increased in embryos co-injected with subcritical doses of *nipblb*-MO and *NPMc+ (I)* in comparison to the control and sub-*nipblb*-MO or sub-*NPMc+* injected embryos *(F-H)*. *(J)* Quantification of the embryos presenting a *spi1b* increased expression. Images were processed as described in Supplementary Methods. Scale bar represents 100 μm. Asterisks in *(E)* represent ***=p<0.001, *(J)* represent **=p<0.01. MO: morpholino; GFP: Green Fluorescent Protein; CHT: Caudal Hematopoietic Tissue; WISH: Whole Mount In Situ Hybridization.

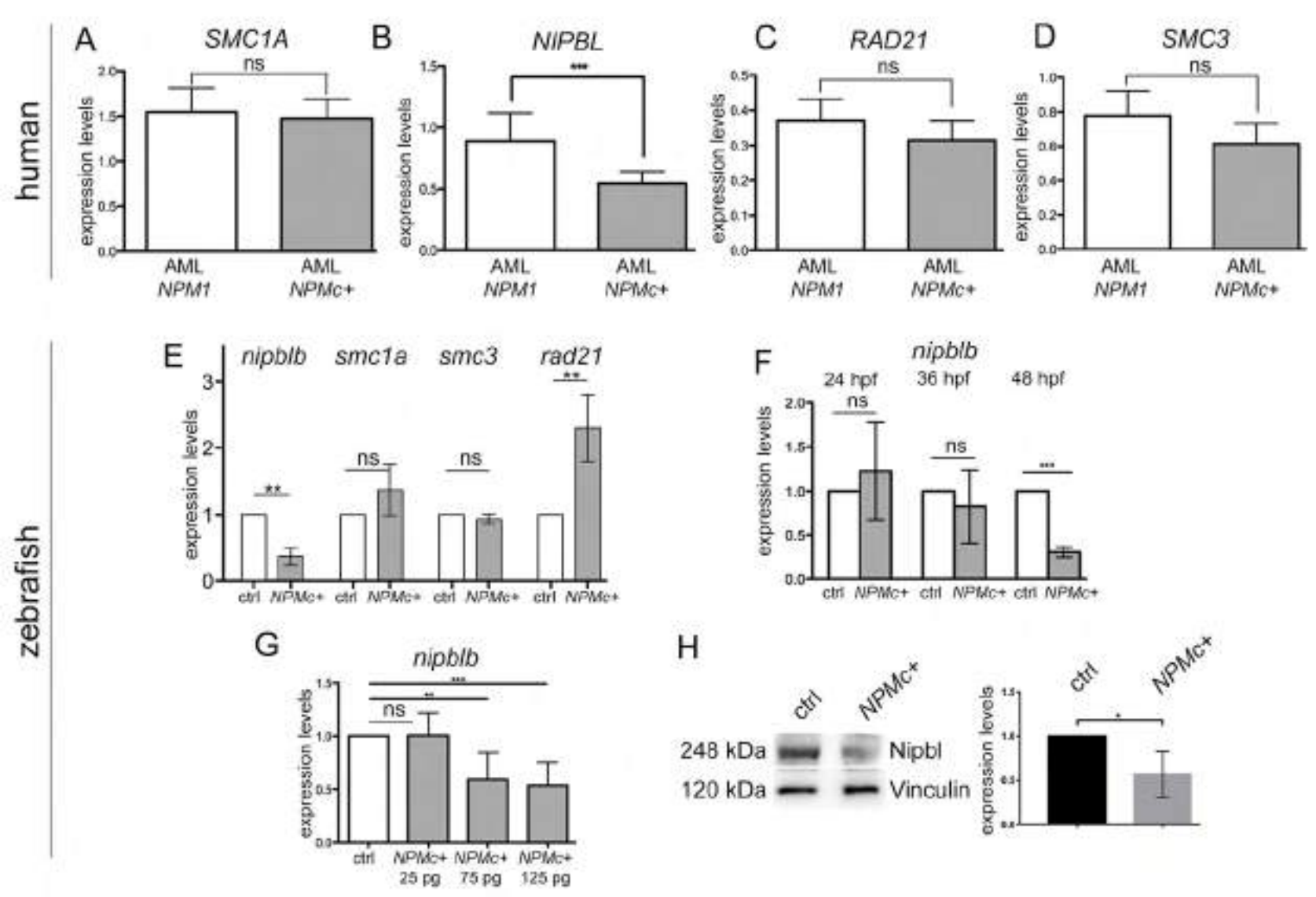
human
A
SMC1A
ns
expression levels
AML NPM1
AML NPMc+
B
NIPBL
***
C
RAD21
ns
D
SMC3
ns
zebrafish
E
nipblb
smc1a
smc3
rad21
**
ns
ns
**
ctrl
NPMc+
F
nipblb
24 hpf
36 hpf
48 hpf
ns
ns
***
G
nipblb
ns
**
***
ctrl
NPMc+ 25 pg
NPMc+ 75 pg
NPMc+ 125 pg
H
ctrl
NPMc+
248 kDa
Nipbl
120 kDa
Vinculin
*

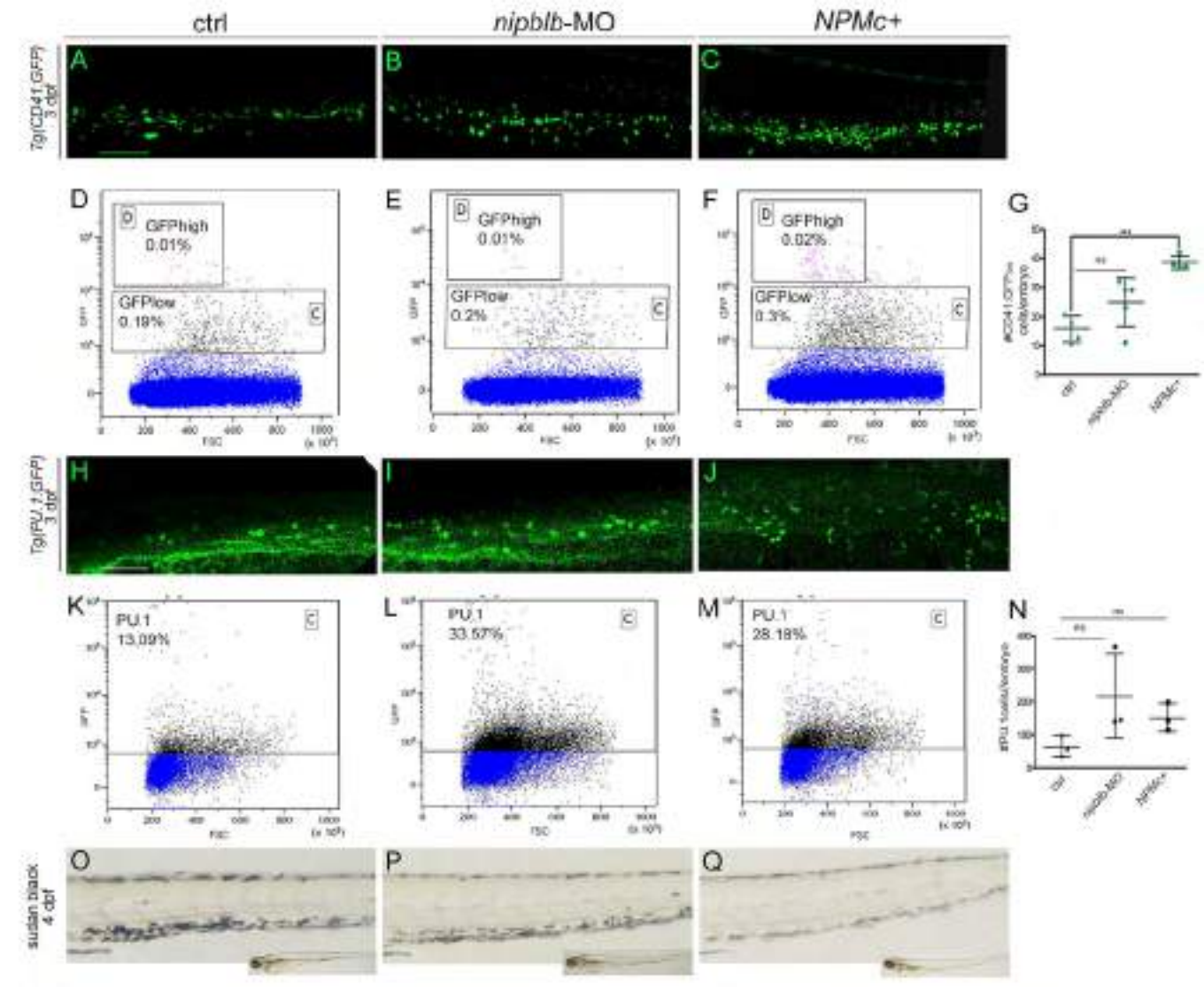
ctrl
nipblb-MO
NPMc+
Tg(CD41:GFP) 3 dpf
A
B
C
D
GFPhigh 0.01%
GFPlow 0.19%
E
GFPhigh 0.01%
GFPlow 0.2%
F
GFPhigh 0.02%
GFPlow 0.3%
G
Tg(PU.1:GFP) 3 dpf
H
I
J
K
PU.1 13.09%
L
PU.1 33.57%
M
PU.1 28.18%
N
sudan black 4 dpf
O
P
Q

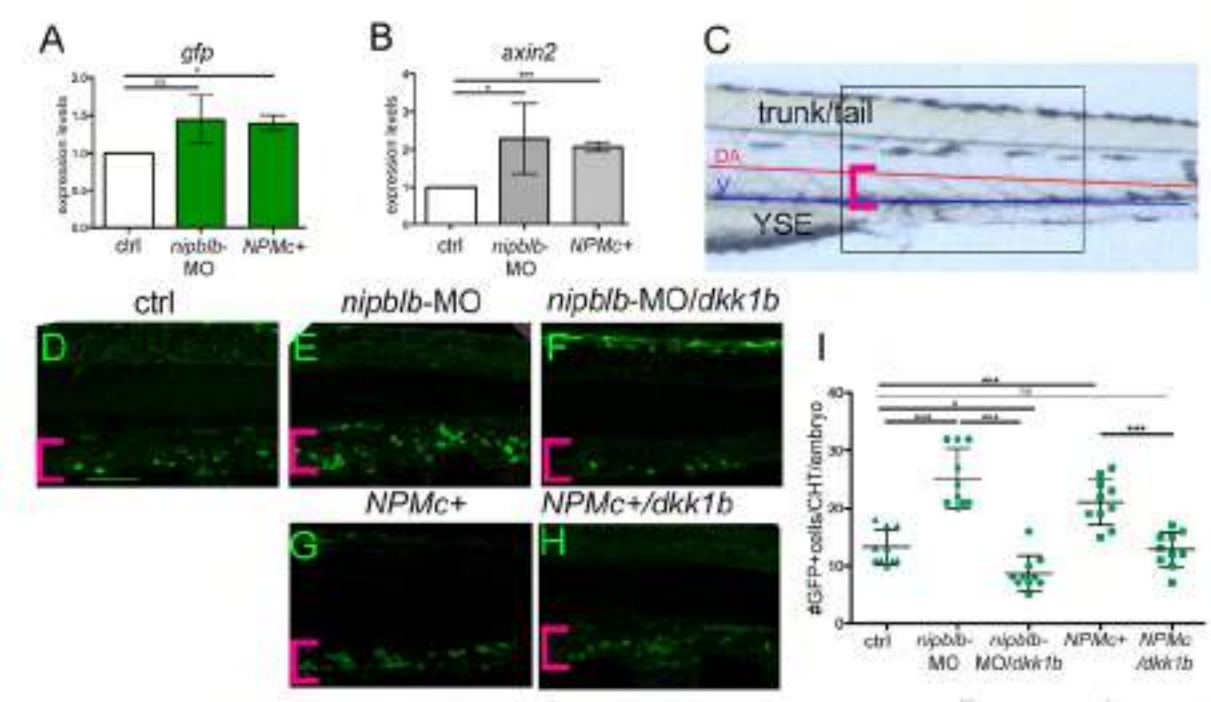
A
gfp
expression levels
ctrl
nipblb-MO
NPMc+
B
axin2
expression levels
ctrl
nipblb-MO
NPMc+
C
trunk/tail
DA
V
YSE
ctrl
nipblb-MO
nipblb-MO/dkk1b
D
E
F
NPMc+
NPMc+/dkk1b
G
H
I
#GFP+cells/CHT/embryo
ctrl
nipblb-MO
nipblb-MO/dkk1b
NPMc+
NPMc /dkk1b

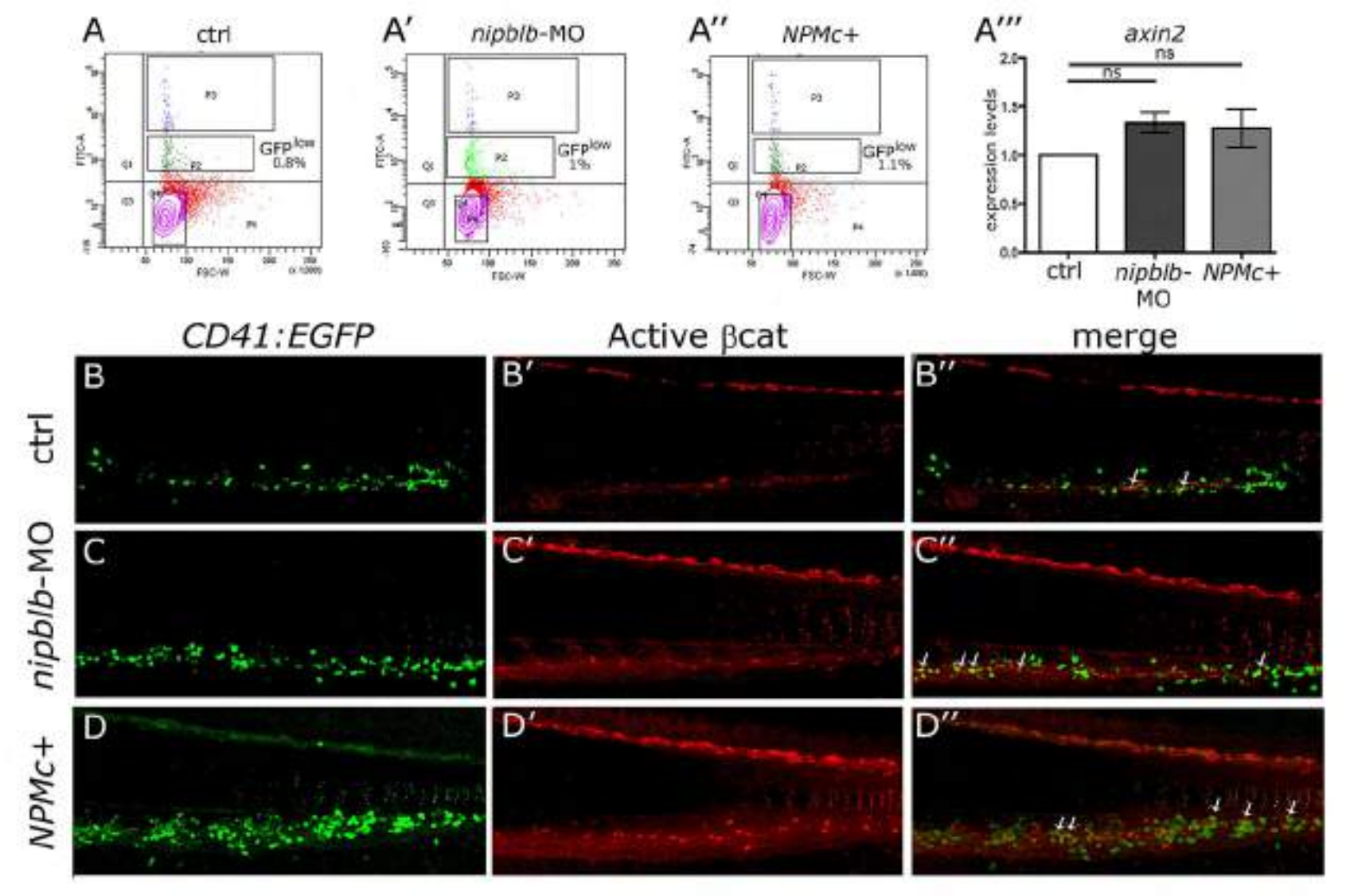
A
ctrl
GFP^low 0.8%
A′
nipblb-MO
GFP^low 1%
A″
NPMc+
GFP^low 1.1%
A‴
axin2
ns
ns
expression levels
ctrl
nipblb-MO
NPMc+
CD41:EGFP
Active βcat
merge
B
B′
B″
C
C′
C″
D
D′
D″
ctrl
nipblb-MO
NPMc+

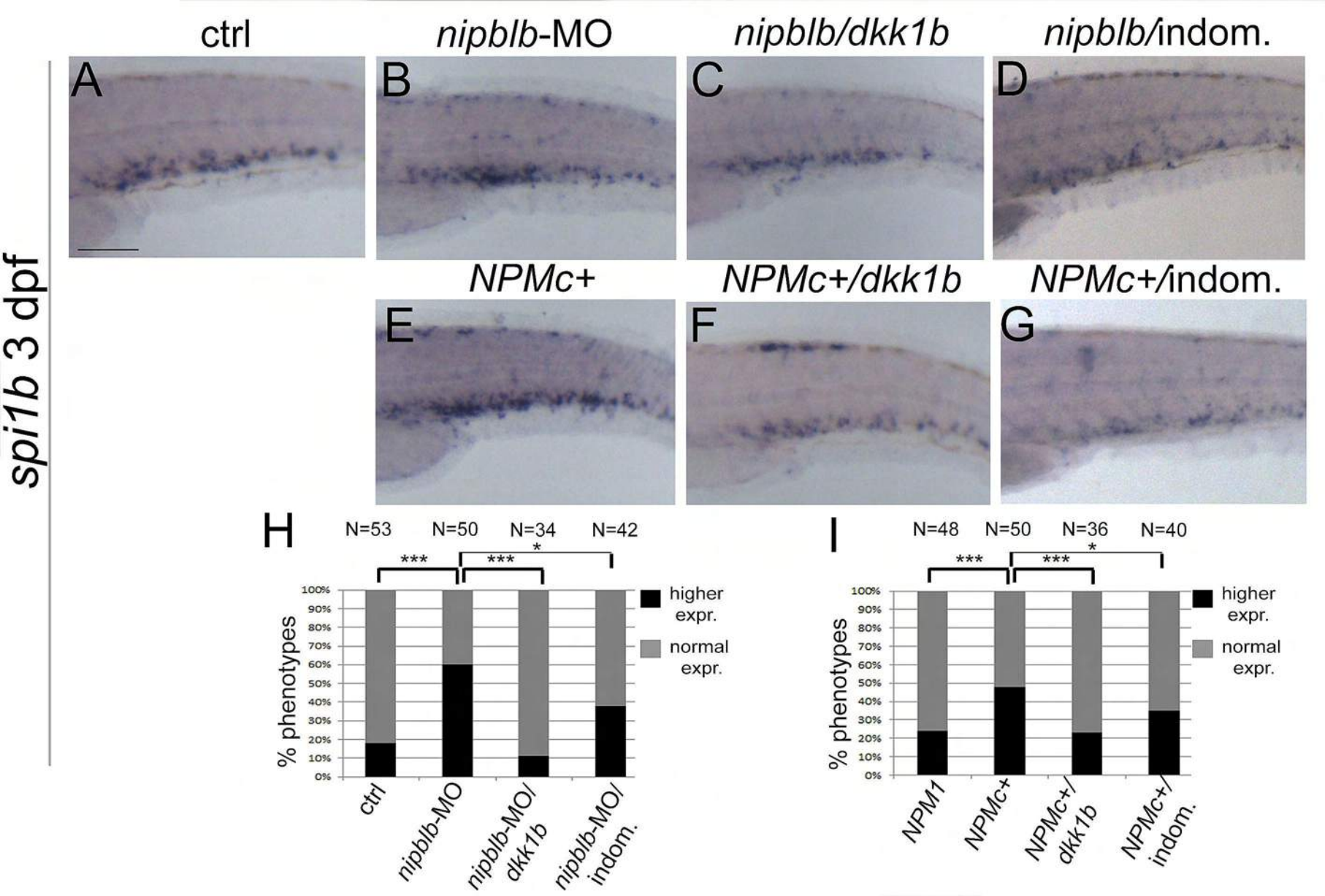
ctrl
nipblb-MO
nipblb/dkk1b
nipblb/indom.
spi1b 3 dpf
A
B
C
D
NPMc+
NPMc+/dkk1b
NPMc+/indom.
E
F
G
H
N=53
N=50
N=34
N=42
***
***
*
100%
90%
80%
70%
60%
50%
40%
30%
20%
10%
0%
% phenotypes
higher expr.
normal expr.
ctrl
nipblb-MO
nipblb-MO/ dkk1b
nipblb-MO/ indom.
I
N=48
N=50
N=36
N=40
***
***
*
NPM1
NPMc+
NPMc+/ dkk1b
NPMc+/ indom.

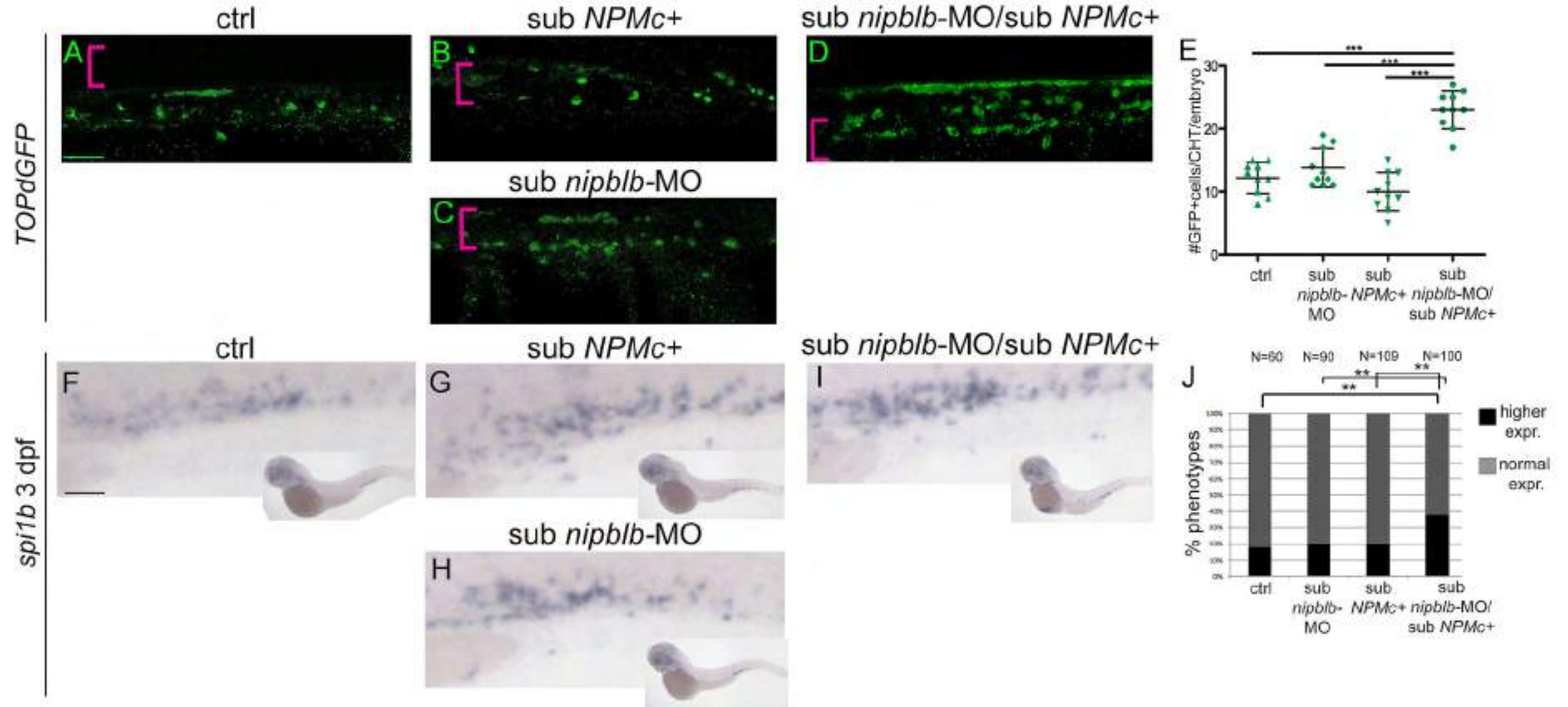
TOPdGFP
ctrl
A
sub NPMc+
B
sub nipblb-MO
C
sub nipblb-MO/sub NPMc+
D
E
#GFP+cells/CHT/embryo
30
20
10
0
***
***
***
ctrl
sub nipblb-MO
sub NPMc+
sub nipblb-MO/ sub NPMc+
spi1b 3 dpf
ctrl
F
sub NPMc+
G
sub nipblb-MO
H
sub nipblb-MO/sub NPMc+
I
J
N=60
N=90
N=109
N=100
**
**
**
% phenotypes
higher expr.
normal expr.
ctrl
sub nipblb-MO
sub NPMc+
sub nipblb-MO/ sub NPMc+

NIPBL: a new player in myeloid cells differentiation

Mara Mazzola[1], Gianluca Deflorian[2], Alex Pezzotta[1], Laura Ferrari[2], Grazia Fazio[3], Erica Bresciani[4], Claudia Saitta[3], Luca Ferrari[1], Monica Fumagalli[5], Matteo Parma[5], Federica Marasca[6], Beatrice Bodega[6], Paola Riva[1], Franco Cotelli[7], Andrea Biondi[3], Anna Marozzi[1], Gianni Cazzaniga[3] and Anna Pistocchi[1]

[1]Dipartimento di Biotecnologie Mediche e Medicina Traslazionale, Università degli Studi di Milano, L.I.T.A., Segrate (MI), Italy.

[2] Istituto FIRC di Oncologia Molecolare, IFOM, Milano, Italy.

[3] Centro Ricerca Tettamanti, Clinica Pediatrica Università di Milano-Bicocca, Centro Maria Letizia Verga, Monza (MB), Italy.

[4] Oncogenesis and Development Section, National Human Genome Research Institute, National Institutes of Health, Bethesda, MD, USA.

[5] Haematology Division and BMT Unit, Ospedale San Gerardo, Monza (MB), Italy.

[6] Istituto Nazionale di Genetica Molecolare "Romeo ed Enrica Invernizzi" (INGM), Milan, Italy.

[7]Dipartimento di Bioscienze, Università degli Studi di Milano, Milano, Italy.

Statement of equal authors' contribution: M.M. and G.D.F. equally contributed to this work

Running head: *NIPBL*/*NPMc+* interplay in myeloid differentiation

Correspondence: Anna Pistocchi: anna.pistocchi@unimi.it

Supplementary Methods

Patients

Patients were previously characterized for specific molecular aberrancies, such as mutations for *NPM1* and *FLT3-ITD*, in addition to translocations t(9;22), t(8;21) and inv(16), in accordance to specific clinical protocol requirements. Patients enrolled belong to different French–American–British (FAB) classification systems (FABs), excluding M3, therefore all patients were negative for translocation t(15;17). BM of were collected as controls for gene expression assays, upon appropriate Informed Consent ASG-MA-052A approved on May 8th 2012 by Azienda San Gerardo (ASG).

Animals

The fish were maintained under standard conditions in the fish facilities of Bioscience Dept, University of Milan, Via Celoria 26 - 20133 Milan, Italy (Aut. Prot, n. 295/2012-A - 20/12/2012); and Cogentech s.c.a.r.l. (Aut. Prot. n. 007894 - 29/05/2018), via Adamello 16 - 20139 Milan, Italy). We express the embryonic ages in hours post fertilization (hpf) and days post fertilization (dpf). Zebrafish AB strains obtained from the Wilson lab (University College London, London, UK) were maintained at 28°C on a 14 h light/10 h dark cycle. The zebrafish transgenic *TOPdGFP* line was described previously.[1] The zebrafish transgenic *CD41:GFP/kdrl:dsRED* line was described previously.[2] Embryos were collected by natural spawning, staged according to Kimmel and colleagues,[3] and raised at 28°C in fish water (Instant Ocean, 0,1% Methylene Blue) in Petri dishes, according to established techniques. After 24 hpf, to prevent pigmentation 0,003% 1-phenyl-2-thiourea (PTU, Sigma-Aldrich, Saint Louis, MO, USA) was added to the fish water. Embryos were washed, dechorionated and anaesthetized, with 0.016% tricaine (Ethyl 3-aminobenzoate methanesulfonate salt; Sigma-Aldrich), before observations and picture acquisitions.

Reverse transcription-PCR and real-time quantitative-PCR assays

For human sample RT-qPCR experiments, Superscript II enzyme (Life Technologies) was used for cDNA synthesis. For this set of experiments, a Light Cycler 480II (Roche Diagnostics, Basel, Swiss) was used. Primers and probes were selected according to the Software Probe Finder (Roche Diagnostics) and are reported in Supplementary Table S2. *hGUS* gene was used as reference and healthy patients cells as standard control. After DNase I RNase-free (Roche Diagnostics) treatment to avoid possible genomic contamination, 1μg of RNA was reverse-transcribed using the "ImProm-II™ Reverse Transcription System" (Promega, Madison, Wisconsin USA) and a mixture of oligo(dT) and random primers according to manufacturer's instructions. RT-qPCRs were carried out in a total volume of 20 μl containing 1X iQ SYBR Green Super Mix (Promega), using proper amount of the RT reaction. RT-qPCRs were performed using the BioRad iCycler iQ Real Time Detection System (BioRad, Hercules, CA, USA). For normalization purposes, rpl8 expression levels[4] were tested in parallel with the gene of interest. Expression levels in the Y axis were relative to the control.

Western Blotting

At least 30 zebrafish embryos were used for protein preparation and the yolk was previously removed from embryos to avoid yolk protein contamination. Protein extracts were classically prepared in RIPA buffer (50 mM Tris-HCl pH 7.4, 1% NP-40, 150 mM NaCl, 0.25% sodium deoxycholate, 1mM EDTA, 1mM PMSF, protease inhibitors Roche) (2 μl/embryo or 1μl/ tail). The protein concentration was determined using a Quantum Micro BCA protein assay kit according to the manufacturer's instructions (Euroclone, Pero, MI, Italy). 30-40 μg of each sample were loaded onto a 7.5% or 10% polyacrylamide gels and subjected to electrophoresis. The proteins were then transferred onto PVDF membranes which were blocked using a blocking solution at room temperature for 1 hour prior to incubation with the primary antibodies: Nipbl (anti rabbit 1:200, Novus Biologicals Littleton, Colorado, USA) and Vinculin (anti mouse 1:6000, Sigma-Aldrich). After incubation with the HRP-conjugated secondary antibodies for 1 h at room temperature (mouse Santa Cruz Biotechnology,

Dallas, TX, USA, rabbit Thermofisher, Waltham, MS, USA), the protein bands were detected using ECL detection systems. Imaging acquisition has been done with the Alliance MINI HD9 AUTO Western Blot Imaging System (UVItec Limited, Cambridge) and analyzed with the related software. Images were processed using the Adobe Photoshop software and when necessary, different parts of the same image have been took separately and later merged in a single image.

In situ *hybridization and immunofluorescent analyses.*

For quantification of the observed phenotypes, WISH experiments were done at least in 2 batches of embryos (minimum 15-20 embryos for each category). Embryos were fixed overnight in 4% paraformaldehyde (Sigma-Aldrich) in Phosphate Buffer Saline (PBS) at 4 °C, then dehydrated stepwise to methanol and stored at −20 °C. Antisense riboprobes were previously *in vitro* labelled with modified nucleotides (*i.e.* digoxigenin, fluorescein, Roche Diagnostics). *cmyb* and *spi1b* probes have been previously described (*myl7*, Zebrafish Information Network[5]). Primary antibody was anti-GFP (1:1000, Torrey Pines Biolab, Houston, TX, USA), anti Active-βcat (Clone 8E7, 1:50 Merck, Darmstadt, Germany) and anti PU.1 (1:100, Merck); the secondary antibodies was Alexa 488-conjugated goat anti-rabbit IgG and Alexa 546-conjugated goat anti-mouse IgG (1:400, Invitrogen Life Technologies, Carlsbad, CA, USA). Images were acquired as described in using a microscope equipped with a digital camera with LAS Leica imaging software (Leica). Images were processed using the Adobe Photoshop software and when necessary, different focal images planes of the same image have been took separately and later merged in a single image.

Sudan Black staining

Embryos were fixed with 4% PFA-PBS for 2 hours at room temperature, rinsed in PBS, incubated in Sudan Black (Sigma-Aldrich) for 20 minutes, washed in 70% ethanol in water, then rehydrated to PBS+0.1% Tween 20 (PBT).

FACS analyses

Embryos were anesthetized with 1X Tricaine/E3 and dissociated with 0.25% trypsin-EDTA (Ethylenediaminetetraacetic acid) and Collagenase from Clostridium (Sigma-Aldrich C9891) 100mg/ml (500 µl dissociation mix/tube of embryos) by pipetting. 1 ml of DMEM (Dulbecco's modified of Eagle medium)-10% FBS (fetal bovine serum) was added and centrifuged 5' at 3000 rpm. Dissociated cells were washed twice in PBS 1X, filtered through 70 µm nylon mesh and transferred into a FACS (Fluorescence-activated cell sorting) tube. For Pu.1 staining, cells were harvested as described above and incubated for 20' on ice in PBS 1X and formaldehyde 2%, washed in PBS 1X + 1% BSA (bovine serum albumin), resuspended in 100 µl TritonX100 0.1 % in PBS 1X and incubated 10' at room temperature. Then, cells were washed once in PBS 1X + 1% BSA and incubated for 45' at 4°C in BSA 5% in PBS 1X. Cells were spinned-down and the pellet was resuspended in 100 µl of anti PU.1 (1:100, Merck) diluted in PBS 1X + 1% BSA and incubated for 1 hour at room temperature, washed once in PBS 1X + 1% BSA; the secondary antibody was Alexa 488-conjugated goat anti-rabbit IgG (1:400, Invitrogen Life Technologie) diluted in PBS 1X + 1% BSA and incubated for 1 hour at room temperature. The pellet was washed and kept stained at 4°C until FACS analysis.

FACS sorting, RNA extraction and cDNA synthesis of GFP low cells

To sort the low and high GFP positive cells, 40 embryos for control, *nipblb*-MO and *NPMc*+ mRNA condition were collected and dissociated as in[6], suspended in 0.4 ml of PBS and sorted with the FACSAria cell sorter. GFP low positive cells were subjected to TRIZOL extraction following manufacturer instruction a resuspended in 5 uL of Nuclease free water. Half of the RNA obtained was used for retro-transcription using Superscript IV VILO. In retro-transcription procedure, EzDNAse digestion step has been included, time of reverse transcription was increased to 30 minutes.

Injections

Two different morpholino against *nipblb*: the ATG-*nipblb*-MO (*nipblb*-MO) and the 5'UTR-*nibpblb*-MO (5UTR*nibpblb*-MO) were used (Gene Tools LLC, Philomath, OR, USA) both previously described and validated.[7] *nipblb*-MO was injected at the concentration of 1 pmol/embryo in 1x Danieau buffer (pH 7,6) for full dose experiments, and at a concentration of 0,6 pmol/embryo for subcritical doses. 5UTR*nibpblb*-MO was injected at the concentration of 0,5 pmol/embryo in 1x Danieau buffer (pH 7,6) for full dose experiments, and at a concentration of 0,3 pmol/embryo for subcritical doses. As a control, we injected a standard control morpholino oligonucleotide (ctrl-MO, Gene Tools). Human *NPM1* and *NPMc+* and zebrafish *dkk1b* mRNAs were injected at the following concentrations: 120 pg/embryo of *NPM1* mRNA, 100 pg/embryo of *NPMc+* mRNA and 50 pg/embryo of *dkk1b* mRNA. For dose-depended assays, *NPMc+* mRNA was injected at 25-75 and 125 pg/embryo. For subcritical doses, *NPMc+* was injected at 50 pg/embryo.

Statistical analyses

For RT-qPCR experiments, data were statistically analyzed applying a two-tailed t-test setting $p \leq 0.05$ (*), $p \leq 0.01$ (**), and $p \leq 0{,}001$ (***) as significant.[27] Data were analyzed using the comparative ΔΔCt method both t test and SD values refer to samples triplicates. In zebrafish at least three different experiments were done for each analysis. For cell count and phenotypical analyses, statistical analysis was performed by Chi square test, with Yates correction when needed.

Supplementary References

1. Dorsky RI, Sheldahl LC, Moon RT. A Transgenic Lef1/β-Catenin-Dependent Reporter Is Expressed in Spatially Restricted Domains throughout Zebrafish Development. Dev Biol 2002;241(2):229–237.
2. Lin HF, Traver D, Zhu H, et al. Analysis of thrombocyte development in CD41-GFP transgenic zebrafish. Blood 2005;106(12):3803–3810.

3. Kimmel C, Ballard W, Kimmel S, Ullmann B, Schilling T. Stages of embryonic development of the zebrafish. Dev Dyn 1995;203(3):253–310.
4. Casadei R, Pelleri MC, Vitale L, et al. Identification of housekeeping genes suitable for gene expression analysis in the zebrafish. Gene Expr Patterns 2011;11(3–4):271–276.
5. Hsu K, Traver D, Kutok JL, et al. The pu.1 promoter drives myeloid gene expression in zebrafish. Blood 2004;104(5):1291–1297.
6. Bresciani E, Broadbridge E LP. An efficient dissociation protocol for generation of single cell suspension from zebrafish embryos and larvae. MethodsX 2018;10(5):1287–1290.
7. Pistocchi A, Fazio G, Cereda A, et al. Cornelia de Lange Syndrome: NIPBL haploinsufficiency downregulates canonical Wnt pathway in zebrafish embryos and patients fibroblasts. Cell Death Dis;4(10):.

Supplementary Figure Legends and Tables

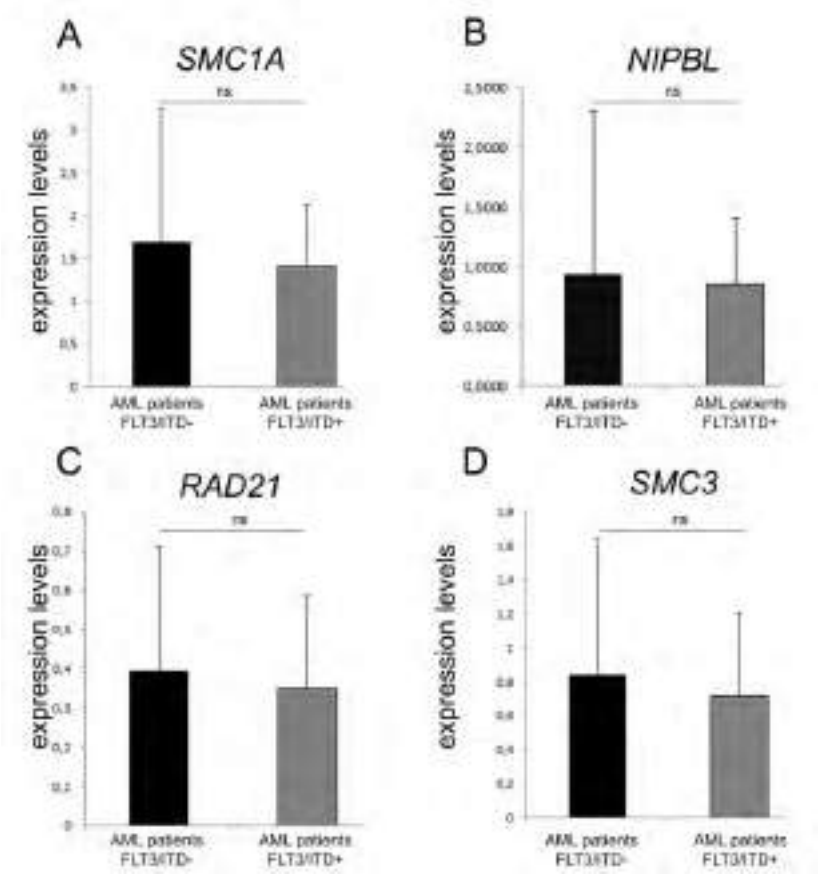

Suppl. Figure S1: Expression analyses of cohesin genes in AML adult patient Bone Marrow samples divided in two subgroups for the absence/presence of *FLT3/ITD* mutations. *(A-D)* RT-qPCR analyses in AML adult patients indicated that the expression level of cohesin genes analyzed was not modified with *FLT3/ITD* mutation. ns: non-significant; AML: Acute Myeloid Leukemia, RT: Retro Transcription.

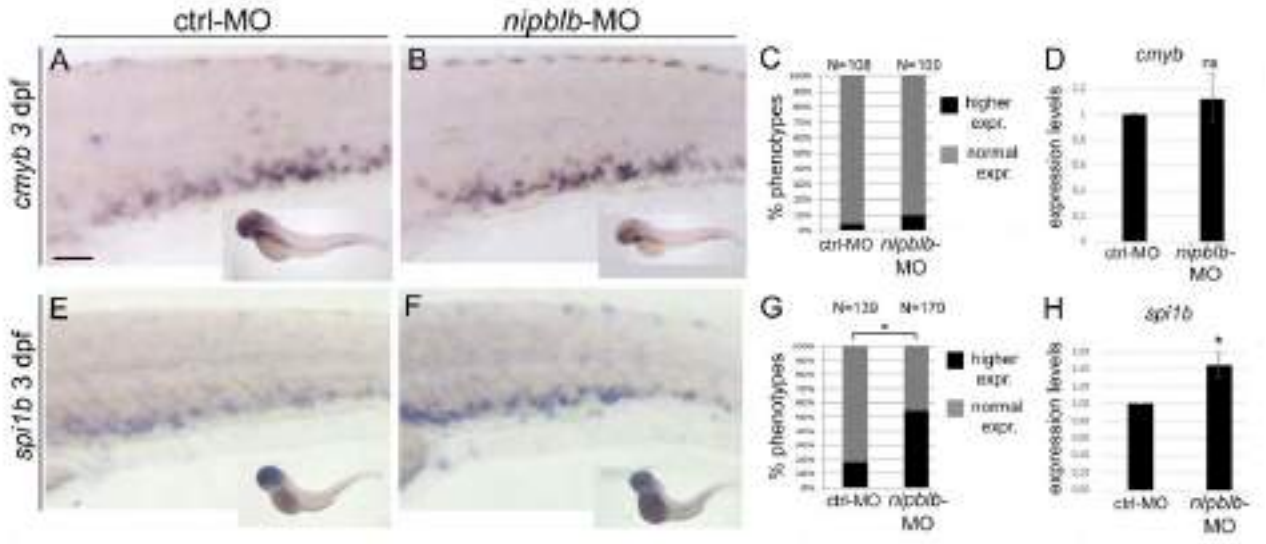

Suppl. Figure S2: Myeloid cell differentiation is affected in *nipblb*-loss-of-function embryos. *(A-B, E-F)* WISH analyses of *cmyb*, marker of HSCs and *spi1b*, marker of myeloid precursors at 3 dpf. *(A-D)* The expression of *cmyb* was comparable in *nipblb*-MO-injected embryos *(B)* and controls *(A);* quantification of the observed phenotypes in *(C)*. RT-qPCR analyses of *cmyb* expression were performed on the tails of the embryos at 3 dpf *(D)*. *(E-H)* The expression of *spi1b* was increased in *nipblb*-MO-injected embryos *(F)* in comparison to controls *(E);* quantification of the observed phenotypes in *(G)*. RT-qPCR analyses of *spi1b* expression were performed on the tails of the embryos at 3 dpf *(H)*. Scale bar represents 100 μm. Asterisks in *(G* and *H)* represent *=p<0.05. ns: non-significant; WISH: Whole Mount In Situ Hybridization; MO: morpholino; RT: Retro Transcription.

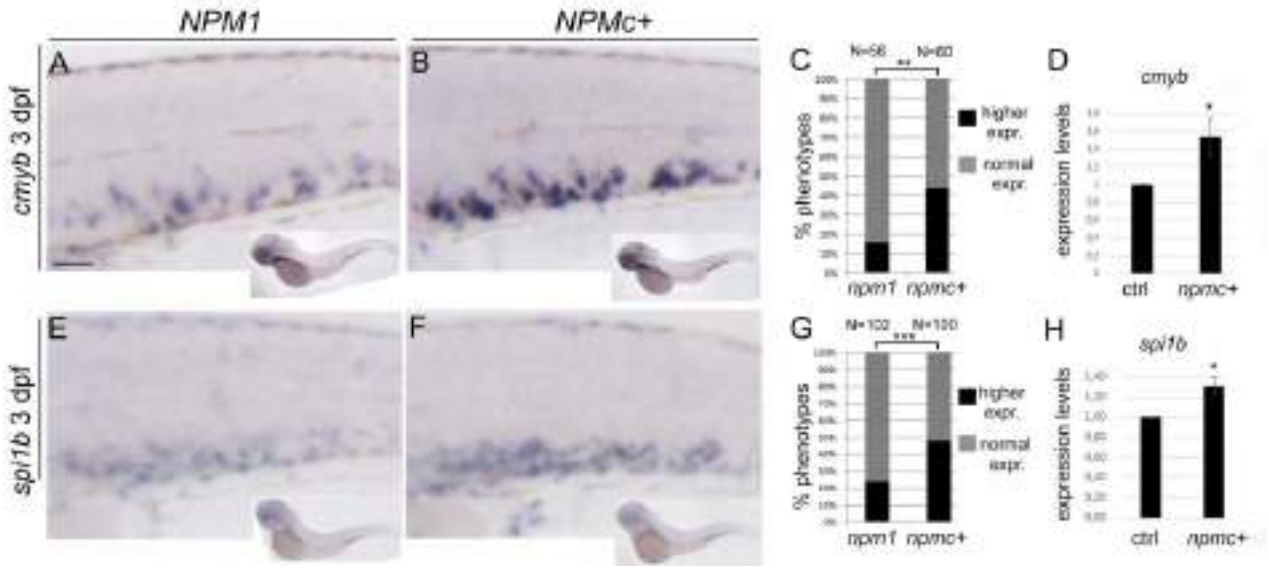

Suppl. Figure S3: HSCs and myeloid cell differentiation are affected in *NPMc+* injected embryos. *(A-B)* WISH analyses of *cmyb*, marker of HSCs, *(E-F) spi1b*, marker of myeloid precursors. The expression of *cmyb* and *spi1b* were increased in *NPMc+*-injected embryos *(B)* and *(F)* in comparison to controls *(A)* and *(E);* quantification of the observed phenotypes in *(C-G).* RT-qPCR analyses of *cmyb* expression *(D)*, and *spi1b* expression *(H)*, were performed on the tails of the embryos. Scale bar represents 100 μm. Asterisks in *(D-H)* represents *=p<0.05, in *(C)* **=p<0.01 and in *(G)* ***=p<0.001. WISH: Whole Mount In Situ Hybridization; MO: morpholino; RT: Retro Transcription.

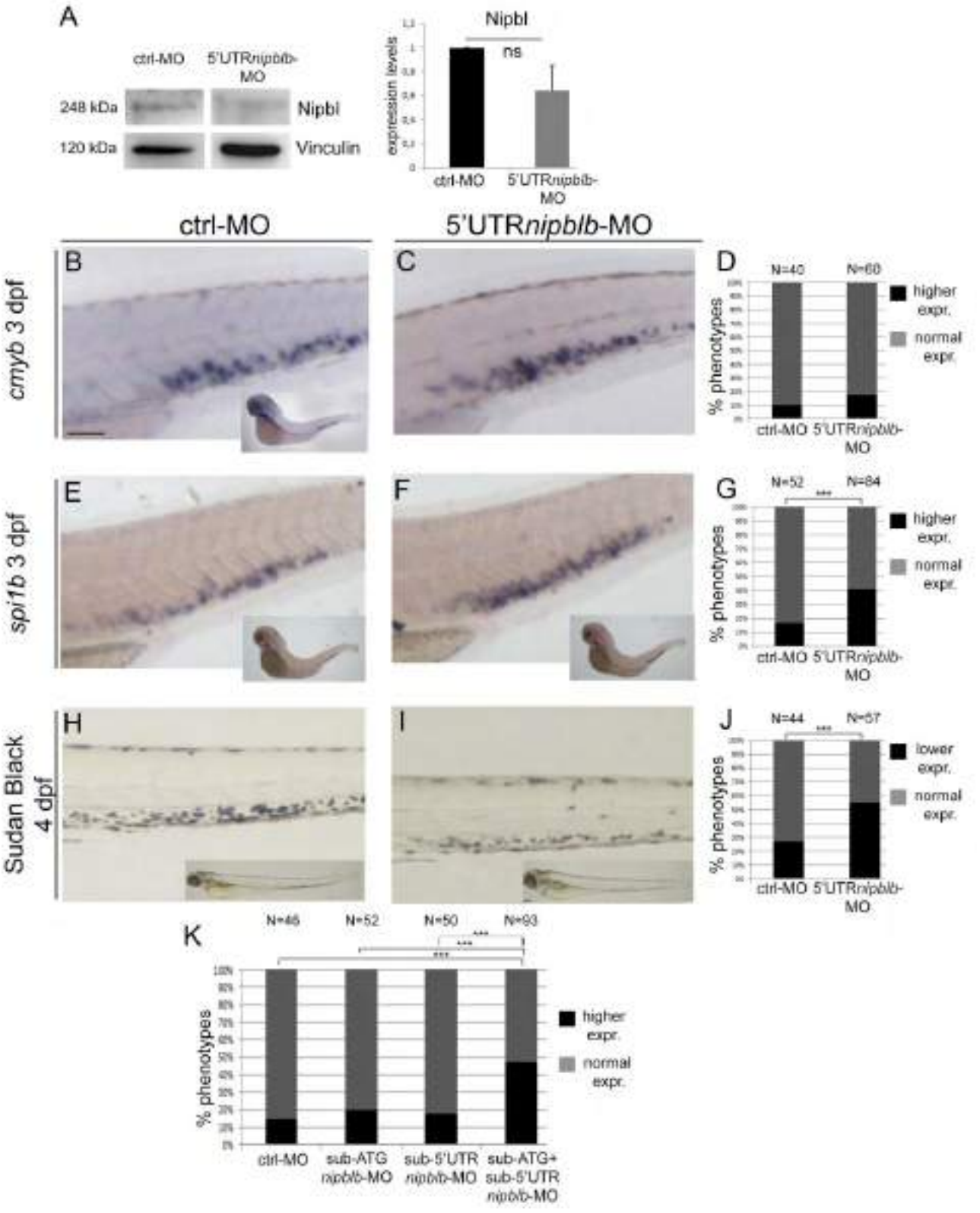

Suppl. Figure S4: Myeloid cell differentiation is affected in 5'UTR*nipblb*-loss-of-function embryos. *(A)* Western blot analyses, repeated twice, of Nipbl protein expression in embryos at 24 hpf injected with 5'UTR*nipblb*-MO. Vinculin marker was used for normalization. *(B, C, E, F)* WISH analyses of *cmyb*, marker of HSCs *(B-C)* and *spi1b*, marker of myeloid precursors *(E-F)*. The

expression of *cmyb* was comparable in 5'UTR*nipblb*-MO-injected embryos *(C)* and controls *(B);* quantification of the observed phenotypes in *(D)*. The expression of *spi1b* was increased in 5'UTR*nipblb*-MO-injected embryos *(F)* in comparison to controls *(E);* quantification of the observed phenotypes in *(G)*. *(H-I)* Sudan black staining of mature myeloid cells of controls. The mature myeloid cells were diminished in 5'UTR*nipblb*-MO injected embryos *(I)* in comparison to controls *(H);* quantification of the observed phenotypes in *(J)*. *(K)* Quantification of embryos with increased number of myeloid precursor cells positive for *spi1b*. The co-injection of subcritical doses of the two morpholinos against *niplbl*, but not that of the single morpholino, recapitulated the myeloid phenotype observed with the injection of morpholino full doses. Scale bar represents 100 μm. Asterisks in *(G, J, K)* represent ***=p<0.001. ns: non-significant; UTR: UnTranslated Region; WISH: Whole Mount In Situ Hybridization; MO: morpholino; HSCs: Hematopoietic Stem Cells; RT: Retro Transcription.

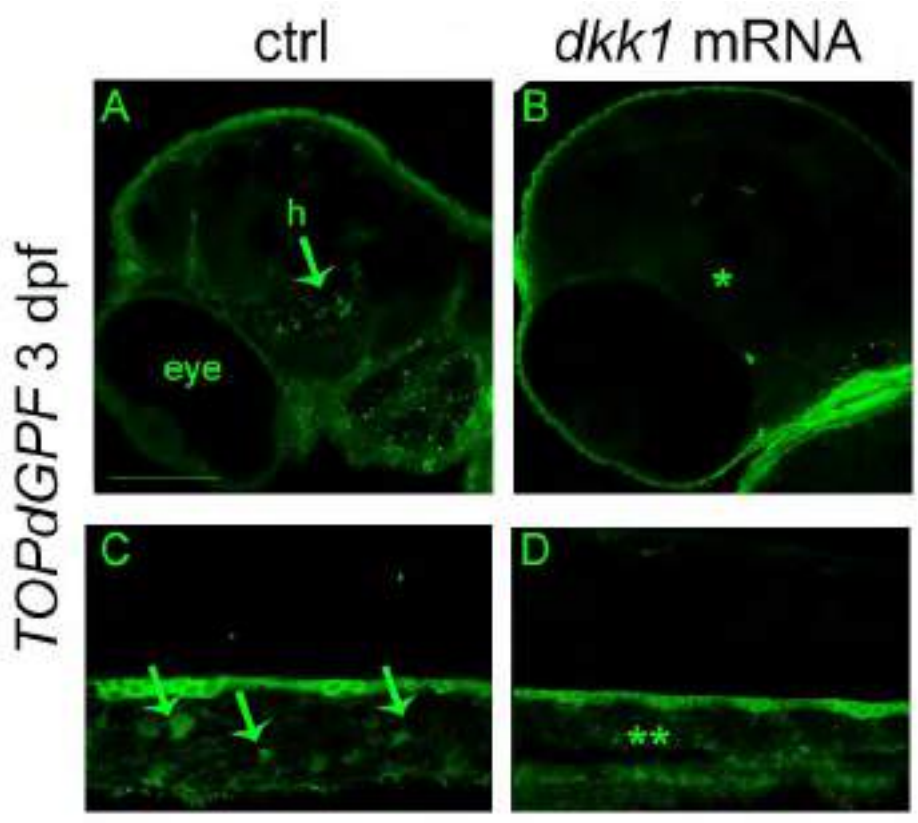

Suppl. Figure S5: Validation of inhibition of canonical Wnt pathway by means of *dkk1b* mRNA injection in the zebrafish Wnt reporter line *TOPdGFP*. *(A-D)* Confocal images of TOPdGFP zebrafish embryos at 3 dpf. The GFP+ cells in the hindbrain (h, arrow) and in the eye of controls *(A)*, were not present in *dkk1b* mRNA injected embryos *(B)*. *(C-D)* Also in the CHT region, the GPF+ cells were absent in *dkk1b* injected embryos *(D)* in comparison to controls *(C)* (arrows). Scale bar represents 100 μm. GFP: Green Fluorescent Protein; CHT: Caudal Hematopoietic Tissue.

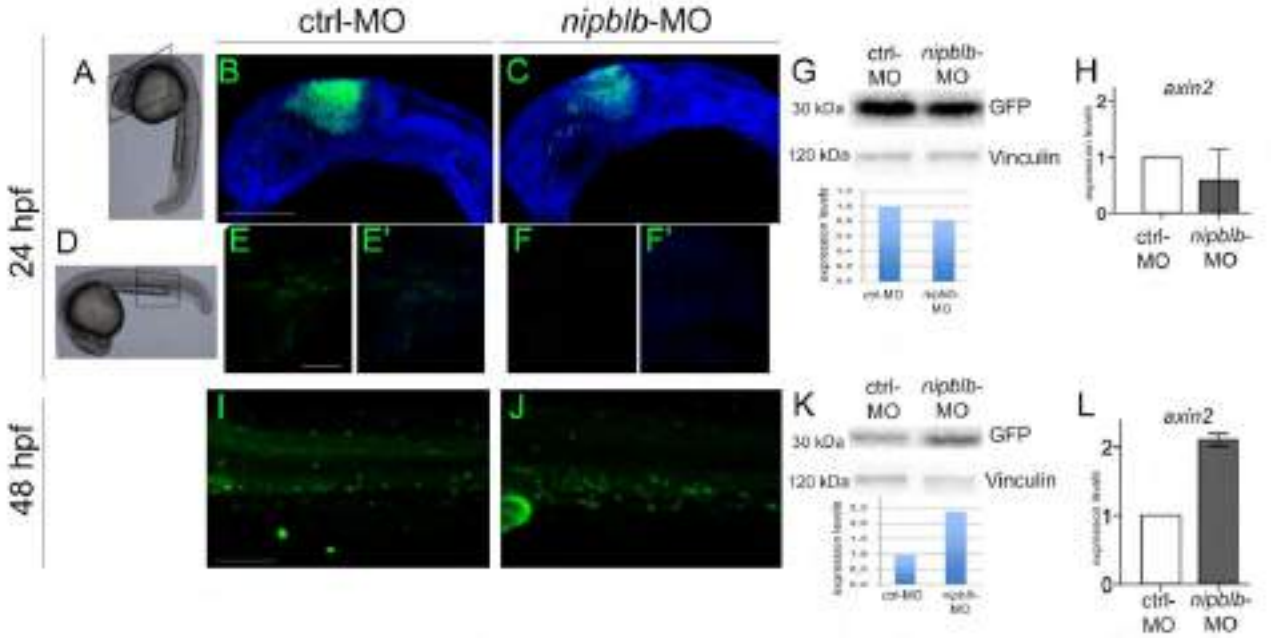

Suppl Figure S6: Different canonical Wnt pathway modulation during zebrafish development following *nipblb* downregulation. *(A-H)* analysis of canonical Wnt pathway activation at 24 hpf in *nipblb*-loss-of-function zebrafish embryos. *(A)* Image of a 24 hpf embryo, the head region was selected for confocal images in *(B-C)*. The GFP expression in the Central Nervous System of TOPdGFP *nipblb*-MO injected embryos *(C)* was decreased in comparison to controls *(B)*. *(D)* Image of a 24 hpf embryo, the Aorta Gonad Mesonephric (AGM) tissue was selected for confocal images in *(E-F')*. The GFP expression of Wnt positive cells in AGM of controls *(E-E')* and *nipblb*-MO injected embryos *(F-F')* was indistinguishable from blood cells autofluorescence at this developmental stages. *(G)* Western blot analyses confirmed the GFP protein reduction in 24 hpf *nipblb*-MO injected embryos in comparison to controls. Vinculin was used as normalizer. *(H)* RT-

qPCR analyses of *axin2* expression, a marker of the status of canonical Wnt pathway. A representative experiment was shown. *(I-L)* Analyses of canonical Wnt pathway activation at 48 hpf. *(I-J)* The GFP expression in the CHT of TOPdGFP *nipblb*-MO injected embryos *(J)* was increased in comparison to controls *(I). (K)* Western blot analyses confirmed the GFP protein increase in 48 hpf *nipblb*-MO injected embryos at in comparison to controls. Vinculin was used as normalizer. *(L)* RT-qPCR analyses of *axin2* expression, a marker of the status of canonical Wnt. DAPI staining was used in *B, C, E', F'*. A representative experiment was shown. Scale bars represent 100 μm. RT-qPCR and Western blot experiment were replicated twice and the data in the figure are the average of the two different experiments. MO: morpholino; GFP: Green Fluorescent Protein; CHT: Caudal Hematopoietic Tissue; RT: Retro Transcription.

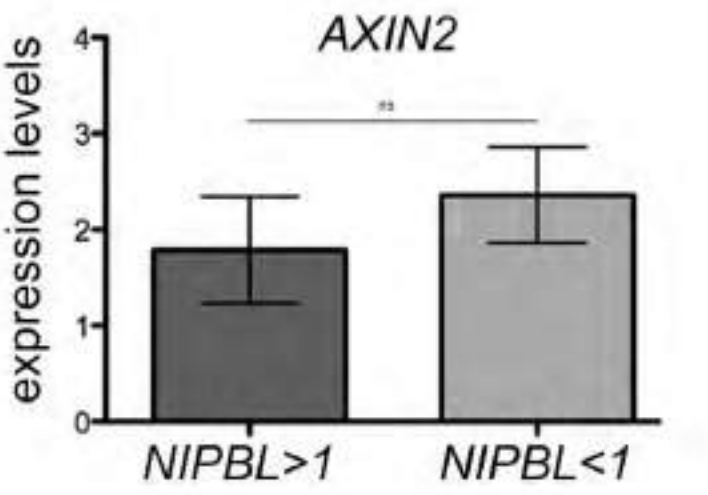

Suppl. Figure S7: *AXIN2* increased expression in AML patients with *NIPBL* downregulation. RT-qPCR analyses of *AXIN2* expression in N=40 AML adult patients divided in two subgroups depending on *NIPBL* expression: *NIPBL*>1 and *NIPBL*<1 in comparison to healthy donors. We did not observe a significant increase in *AXIN2* expression when *NIPBL* was downregulated. ns: non-significant; RT: Retro Transcription.

Suppl. Table S1

Supplementary Table S1. Clinical Features of patients' cohort.								
	AGE AT ONSET	KARYOTYPE	FAB CLASSIFICATION	NPM	FLT3-ITD	t(9;22)	t(8;21)	inv(16)
1	47	46,XX,t(10;11)(p11;p15)[20]	M0	NEG	NEG	NEG	NEG	NEG
2	49	46,XY[20]	M0/M1	NEG	NEG	NEG	NEG	NEG
3	48	46,XX[20]	M1	NEG	NEG	NEG	NEG	NEG
4	70	45,X,-Y,t(8;21)(q22;q22)[5]/46,XY[5]	M2	NEG	NEG	NEG	NEG	NEG
5	72	47,XY,+mar[10]/46,XY[10]	M2	NEG	NEG	NEG	NEG	NEG
6	58	46,XX,t(3;5)(q25;q34)[20]	M2	NEG	NEG	NEG	NEG	NEG
7	70	44~45,XX,?+X,t(1;22)(q12;q11),+1,del(5)(q13q34),?inv(7)(q14q22),tas(8;15)(q24;p13),-17,-21,del(22)(q11)der(22)t(1;22)(q12;q11),+mar[cp18]/45,XX,t(1;22)(q12;q11),+1,del(5)(q13q34),-7,der(17)t(7;17)(q11;q25),-21,del(22)(q11)der(22)t(1;22)(q12;q11)[7]	M4	NEG	NEG	NEG	NEG	NEG
8	48	45,X,-X,t(8;21)(q22;q22)[20]/45,X,-X[3]	M2	NEG	NEG	POS	NEG	NEG
9	47	45-46,XY,del(3)(q?22q?26),der(4)t(?1;4)(p36;p16),add(11)(p14),-12,del(12)(p11),add(21)(q22)[cp13]/46,XY[7]	nk	NEG	NEG	nk	NEG	NEG
10	37	43,XY,?del(2)(q?33),-4,der(6)t(?4;6)(q?22;q21),i(11)(q10),-17,-18[19]/46,XY[2]	M1	NEG	NEG	NEG	nk	nk
11	59	46,XY[20]	nk	NEG	POS	NEG	NEG	NEG
12	33	46,XY[15]	M1	NEG	POS	NEG	NEG	NEG
13	30	46,XY[20]	M5	NEG	POS	nk	NEG	NEG
14	20	46,XY,t(8;21)(q22;q22)[21]/46,XY[1]	nk	NEG	POS	nk	POS	NEG
15	58	46,XY,inv(16)(p13q22)[20]	M4	NEG	POS	nk	POS	NEG
16	76	nk	M5	NEG	POS	nk	NEG	NEG
17	78	46,XX[27]	M4	NEG	POS	nk	NEG	NEG
18	53	46,XY[22]	M4	NEG	POS	nk	NEG	NEG
19	64	46,XX[20]	M5	NEG	POS	nk	NEG	NEG
20	75	46,XY[26]	M4	NEG	POS	nk	NEG	NEG
21	39	46,XY[20]	M1	POS(A)	NEG	NEG	NEG	NEG
22	47	46,XX[20]	M5	POS(A)	NEG	NEG	NEG	NEG
23	63	46,XY,t(8;14)(q24;q32),add(13q34)[18]/46,XY[9]	nk	POS(D)	NEG	nk	NEG	NEG
24	58	46,XY/47,XY,+8[7/10]	nk	POS(QM)	NEG	nk	NEG	NEG
25	50	46,XX[20]	M4	POS(A)	NEG	nk	NEG	NEG
26	77	46,XY[20]	nk	POS(A)	NEG	nk	NEG	NEG
27	54	46,XX,t(9;22)(q34;q11)[14]/46,XX[6]	M4	POS(A)	NEG	POS	NEG	NEG
28	60	46,XX[6]	nk	POS	NEG	nk	NEG	NEG
29	62	46,XX[25]	M5	POS(A)	NEG ITD/POS D835/D836	nk	NEG	NEG
30	58	46,XX[20]	nk	POS(A)	NEG	nk	NEG	NEG
31	48	46,XX[20]	M4	POS(A)	POS	NEG	NEG	NEG
32	51	46,XX[20]	M5	POS(A)	POS	NEG	NEG	NEG
33	68	46,XX[20]	M4	POS(A)	POS ITD/POS D835/D836	NEG	NEG	NEG
34	46	46,XY[20]	M2	POS	POS	NEG	NEG	NEG
35	39	46,XX[22]	M1	POS(A)	POS	nk	NEG	NEG
36	58	46,XY	M5	POS(A)	POS	nk	NEG	NEG
37	35	46,XY,?r(18)(?)[16]/47,idem,+8[3]/46,XY[1]	nk	POS(B)	POS	nk	NEG	NEG
38	58	46,XY[24]	M1	POS(A)	POS	nk	NEG	NEG
39	70	46,XY[20]	M5	POS(A)	POS	nk	NEG	NEG
40	12	46,XY[24]	nk	POS(A)	POS	NEG	NEG	NEG

Suppl. Table S2

Human primers sequence and probe number used in qPCR experiments.			
PRIMER	**lenght**	**sequence**	**PROBE**
hGUS-L	20	CGCCCTGCCTATCTGTATTC	**57**
hGUS-R	20	TCCCCACAGGGAGTGTGTAG	
hNIPBL-L	19	CTATGCGAACAGCCCAAAA	**55**
hNIPBL-R	24	TTCACCTTGCTTACTACCACATTT	
hSMC1A-L	21	CGACATCTAGCCCTGAATCTG	**78**
hSMC1A-R	20	ATTAATGCGAGGCCCAAAGT	
hRAD21-L	20	ATTGACCCAGAGCCTGTGAT	**62**
hRAD21-R	20	GGGGAAGCTCTACAGGTGGT	
hSMC3-L	22	TGCACTGAATGATGAGATTCGT	**18**
hSMC3-L	27	TTAATTCTTTCATTTAGCAACTGTCTG	
hAXIN2-L	19	CCACACCCTTCTCCAATCC	**36**
hAXIN2-R	20	TGCCAGTTTCTTTGGCTCTT	

Suppl. Table S3

Zebrafish primers sequence used in qPCR experiments.		
PRIMER	**lenght**	**sequence**
***zrpl8*-L**	21	CTCCGTCTTCAAAGACCATGT
***zrpl8*-R**	21	TCCTTCACGATCCCCTTGATG
***znipblb*-L**	20	TGGAAGAAAAGACTCCTGGG
***znipblb*-R**	20	ACGTCCGTGGCTTCCACGGT
***zsmc1a*-L**	20	AAATGTGGAGGACGCTCGTA
***zsmc1a*-R**	20	AGGTCACTAGCTCCTCCAGA
***zrad21*-L**	20	AGGAAGGACAGGGAGGAGAT
***zrad21*-R**	20	GTTGTTTCTGCACAGCTCCA
***zsmc3*-L**	20	CCCTTCGGCTCAAAACACAA
***zsmc3*-R**	20	TGGCCGAAGATGACTGAACT
***zspi1b*-L**	19	GCCATTTCATGGACCCAGG
***zspi1b*-R**	19	ACACCGATGTCCGGGGCAA
***zcmyb*-L**	20	GACACAAAGCTGCCCAGTTG
***zcmyb*-R**	20	GCTCTTCCGTCTTCCCACAA

***zaxin2*-F**	20	GGCCACTGTAGTGGGTCTGT
***zaxin2*-R**	20	ATTAGGATTTCCGGGGTCAC

Suppl. Table S4

Antibodies	Specie	Concentration	Technique
Vinculin	mouse	1:6000	WB
NIPBL	rabbit	1:200	WB
Active-βcat	mouse	1:50	IF
Pu.1	rabbit	1:100	IF/FACS
Alexa anti mouse 546	goat	1:400	IF